Atmospheric and Climate Sciences, 2026, 16(3), 628-657
https://www.scirp.org/journal/acs
ISSN Online: 2160-0422
ISSN Print: 2160-0414

Station-Based Characterization of Seasonal Drought across Burkina Faso's Climatic Zones: Insights from SPI-3 and SPEI-3 (1981-2021)

Charouna Compaoré[1]*, Rimyalegdo Kiébré[2], Marcel Bawindsom Kébré[1], Zacharie Koalaga[1]

[1]Laboratoire de Matériaux et Environnement (LA. M. E), Université Joseph Ki-Zerbo, Ouagadougou, Burkina Faso
[2]Département de Physique et Chimie, Université Lédéa Bernard OUEDRAOGO, Ouahigouya, Burkina Faso
Email: *ccharoun20@gmail.com, rkiebre@gmail.com, marcel.kebre@ujkz.bf, zacharie.koalaga@ujkz.bf

How to cite this paper: Compaoré, C., Kiébré, R., Kébré, M.B. and Koalaga, Z. (2026) Station-Based Characterization of Seasonal Drought across Burkina Faso's Climatic Zones: Insights from SPI-3 and SPEI-3 (1981-2021). *Atmospheric and Climate Sciences*, **16**, 628-657.
https://doi.org/10.4236/acs.2026.163032

Received: June 22, 2026
Accepted: July 26, 2026
Published: July 29, 2026

Abstract

This study characterizes seasonal drought variability at nine synoptic stations spanning Burkina Faso's climatic zones over 1981-2021, using the Standardized Precipitation Index (SPI-3) and the Standardized Precipitation Evapotranspiration Index (SPEI-3) computed at nine synoptic stations representative of the country's three climatic zones—Sahelian, Sudano-Sahelian, and Sudanian. A multi-indicator approach combining non-parametric trend analysis (Hamed-Rao modified Mann-Kendall test, Sen's slope) and structural change point detection (Pettitt test) is applied to two intra-seasonal windows: the early rainy season (MJJ: May-June-July) and the late rainy season (ASO: August-September-October). Results reveal three structurally distinct hydroclimatic phases. The period 1981-1990 was dominated by severe and extreme droughts, spatially coherent across all zones and concentrated in the Sahelian sector. A partial rainfall recovery emerged from 1991 onward, consistent with the documented Sahelian re-greening, with significant structural change points clustering in two windows: 1997 and 2007-2009. However, SPEI-3 systematically detects higher moderate and severe drought frequencies than SPI-3 after 2000, revealing an intensification of evapotranspiration-driven water stress decoupled from precipitation trends—particularly in the Sudano-Sahelian zone and at the late-season scale. SPI-3 retains superior sensitivity for extreme drought detection, driven by catastrophic rainfall deficits, while SPEI-3 better captures chronic, low-intensity stress with direct implications for rainfed agriculture. The early season (MJJ) constitutes the primary locus of monsoon onset vulnerability, while the late season (ASO) experiences increasing thermal amplification of drought, particularly in the Sudanian zone. These findings underscore the diagnostic necessity of jointly using SPI-3 and SPEI-3 for drought monitoring in semi-arid West Africa, and provide a spatially differentiated evidence base for climate adaptation strategies in a country where over 80% of the population depends on rainfed agriculture.

Keywords

Meteorological Drought, SPI-3/SPEI-3, Seasonal Variability, Evapotranspiration-Driven Water Stress, Burkina Faso

1. Introduction

Drought is among the most pervasive hydroclimatic hazards in the Sahel, with far-reaching consequences for agricultural productivity, food security, and socio-economic resilience [1] [2]. In the West African Sahel, the 1970s-1980s were marked by some of the most severe and prolonged droughts on record [3], and the World Meteorological Organization (2021) estimated that droughts caused over USD 250 billion in global losses between 1970 and 2019, with Africa accounting for 26% of disaster-related losses during that period. While rainfall has partially recovered since the 2000s—a phenomenon documented as the Sahelian "re-greening"—rising temperatures are simultaneously intensifying potential evapotranspiration, leading to an amplification of water stress even under relatively wet conditions [4]. Beyond climate forcing, anthropogenic pressures—including land-use change, dam construction, and agricultural overexploitation—further exacerbate surface water depletion [5] [6]. In Burkina Faso specifically, recurrent drought years (1972-1973, 1983-1984, 1991, 2004, 2010, 2012) have triggered severe crop failures, large-scale migration, and groundwater depletion, underscoring the urgent need for robust, multi-scale drought monitoring frameworks [7] [8].

Drought is a multidimensional phenomenon typically classified into four cascading types: meteorological, agricultural, hydrological, and socio-economic [9]-[11]. Meteorological drought—driven by precipitation deficits—is the primary trigger, propagating to soil moisture depletion (agricultural drought), then to reduced streamflow and reservoir levels (hydrological drought), and ultimately to societal water shortages [7]. Characterizing drought across these dimensions requires the use of standardized indices that quantify severity, duration, and spatial extent [12]-[14]. Among the most widely applied, the Standardized Precipitation Index (SPI) [15] captures precipitation anomalies at multiple timescales, while the Standardized Precipitation Evapotranspiration Index (SPEI) [16] extends this framework by incorporating the thermal component through potential evapotranspiration (PET). The joint use of both indices is particularly valuable in contexts of climate warming, where the SPI-SPEI divergence can reveal the increasing role of evaporative demand in controlling drought severity [17].

Several studies have investigated drought variability in Burkina Faso and the broader Sahel using standardized indices. [18] analyzed surface water dynamics in the Nakanbé-Mané basin (2000-2020) using SPI and remote sensing indices, revealing a significant declining trend in water surfaces linked to recurrent droughts. At the basin scale, [7] examined the propagation from meteorological to hydrological drought in the Nakanbé River upstream of Wayen (1971-2014), showing that SPI and SPEI at 12-month timescales best predict streamflow anomalies. [19]-[21] further attributed runoff changes in the Sahelian Nakanbé to the combined effects of climate variability and land degradation. At the regional Sahel scale [22] identified three distinct drought-prone clusters using SHAP-driven machine learning applied to SPEI-12, highlighting the dominant role of the Atlantic Multidecadal Oscillation (AMO) in shaping drought dynamics. Despite these advances, several gaps remain. Most Burkina Faso studies do not extend beyond 2014, leaving the 2015-2021 period—characterized by marked hydroclimatic shifts—poorly documented.

This study addresses these gaps by pursuing three complementary objectives: 1) characterizing the spatio-temporal variability of historical meteorological droughts (1981-2021) across nine synoptic stations representative of Burkina Faso's three climatic zones (Sahelian, Sudano-Sahelian, and Sudanian), using the SPI-3 and SPEI-3 indices computed from ANAM in situ data and CHIRPS reanalysis; 2) detecting structural change points and monotonic trends in drought dynamics using the Pettitt test, the modified Mann-Kendall test, and Sen's slope estimator.

2. Materials and Methods

2.1. Study Area and Datasets

Burkina Faso is a landlocked country in West Africa, located in the Sahel region. It has a population of approximately 20 million inhabitants. The country extends from 9.25˚N to 15.01˚N in latitude and from 2.22˚E to 5.32˚W in longitude, with its northern part lying within the Sahelian zone of West Africa [23]. Burkina Faso covers 274,200 km^2 and is characterized by generally flat topography, consisting predominantly of a savanna plateau with elevations ranging from 250 to 400 m (**Figure 1**). Rainfall distribution varies across climatic zones, with annual totals ranging from 500 to 800 mm in the semi-arid north and from 900 to 1200 mm in the tropical savanna regions [23]. Burkina Faso experiences two well-defined seasons: a rainy season extending from early June to late September, and a dry season covering the remainder of the year.

In this study, in situ daily raw records of precipitation and potential evapotranspiration (PET) for the synoptic stations were obtained from ANAM and cover the same historical period (1981-2021). **Figure 1** illustrates the different climatic zones and the locations of the ten synoptic stations of Burkina Faso. However, only nine stations, excluding Bogandé, were retained for the subsequent analyses. Indeed, as documented by [24], Bogandé exhibited substantially higher missing-data rates than the other stations, notably with more than 40% missing values for potential evapotranspiration, whereas missingness for the key variables considered here, particularly precipitation and potential evapotranspiration, remained

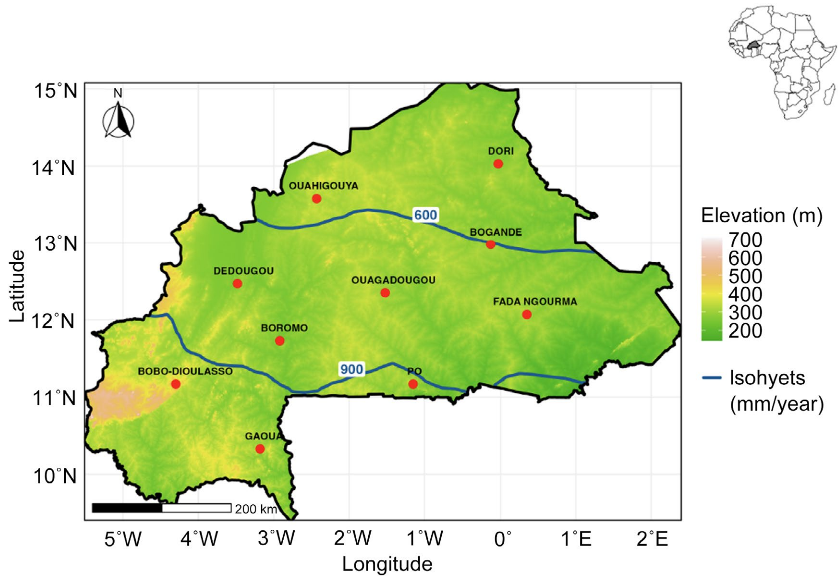

Figure 1. Topography, station network, and climatic zonation of Burkina Faso. Elevation is derived from a digital elevation model (DEM). The nine ANAM synoptic stations analyzed in this study are indicated by filled symbols. Mean annual rainfall isohyets for 1981-2021 (600 and 900 mm/year, based on CHIRPS v2.0) delimit the three climatic zones: Sahelian (<600 mm/year), Sudano-Sahelian (600 - 900 mm/year), and Sudanian (>900 mm/year).

generally low to negligible at the retained stations: missing values for precipitation remained negligible at all retained stations, not exceeding 0.5% in any case, and PET missingness was similarly low, generally below 1.5%, with the sole exception of Pô where it reached 8.1%. These levels of missingness are insufficient to compromise the computation of long-term drought indices over a 41-year record.

Furthermore, a preliminary homogeneity assessment conducted by [24] revealed that precipitation exhibits statistically significant breakpoints at only three stations (Ouagadougou, Dédougou, and Ouahigouya), with break years ranging between 1996 and 2007; these discontinuities may partly reflect genuine hydroclimatic shifts rather than purely instrumental artefacts, given the well-documented post-1990s rainfall recovery across the Sahel. PET breakpoints, detected at six stations, are more likely to reflect the compound effect of changes in its constituent meteorological variables—temperature, humidity, and wind speed—rather than independent instrumental discontinuities, and are therefore not expected to introduce systematic bias into the SPEI-3 computations.

2.2. Computation of SPI and SPEI Indices

2.2.1. Standardized Precipitation Index (SPI)

The SPI was introduced by [15] to quantify precipitation anomalies at multiple timescales. Its widespread adoption stems from its computational transparency, its reliance on a single variable (precipitation), and its ability to characterize both drought onset and termination. In this study, SPI-3 is computed from monthly in situ precipitation records (1981-2021) provided by ANAM, covering the nine synoptic stations. The 41-year baseline (1981-2021) exceeds the 30-year minimum recommended for robust parameter estimation [15].

The SPI is derived through a four-step procedure that transforms raw precipitation accumulations into standardized normal deviates via a gamma probability distribution, as detailed below.

- **Fitting the gamma distribution**

Monthly precipitation accumulations $u > 0$ at each station and timescale k are fitted to the two-parameter Gamma distribution, whose probability density function (PDF) is:

$$g(u) = \frac{1}{\beta^{\alpha}\Gamma(\alpha)} u^{\alpha-1} \exp(-u/\beta) \tag{1}$$

where $\alpha > 0$ is the shape parameter, $\beta > 0$ the scale parameter, u the precipitation amount, and $\Gamma(\alpha)$ the Gamma function:

$$\Gamma(\alpha) = \int_0^{\infty} v^{\alpha-1} \exp(-v) \mathrm{d}v \tag{2}$$

Parameters α and β are estimated using the maximum likelihood approximation proposed by Thom [1966]:

$$\alpha = \frac{1}{4X}\left(1 + \sqrt{1 + \frac{4X}{3}}\right) \tag{3}$$

$$\beta = \frac{\bar{u}}{\alpha} \tag{4}$$

$$X = \ln(\bar{u}) - \frac{1}{n}\sum_i \ln(u_i) \tag{5}$$

where $\bar{u}$ is the sample mean precipitation and n the number of non-zero observations.

- **Cumulative distribution function (CDF)**

The CDF of the fitted Gamma distribution is:

$$G(u) = \int_0^{u} g(t;\alpha,\beta) \mathrm{d}t \tag{6}$$

Because the Gamma distribution is undefined at $u = 0$, and precipitation can be zero, the CDF is adjusted to account for the probability $p = P(u = 0)$ of zero precipitation:

$$H(u) = p - (1-p)G(u) \tag{7}$$

- **Normal quantile transformation (SPI value)**

The SPI value is obtained by transforming $H(u)$ into the corresponding quantile of the standard normal distribution N(0, 1), using the rational approximation of [25]:

$$\mathrm{SPI} = -\left(t - \frac{C_0 + C_1 t + C_2 t^2}{1 + d_1 t + d_2 t^2 + d_3 t^3}\right) \text{ with } t = \sqrt{\ln\left(\frac{1}{H(u)^2}\right)} \text{ for } 0 < H(u) \le 0.50 \tag{8}$$

$$\text{SPI} = +\left(t - \frac{C_0 + C_1 t + C_2 t^2}{1 + d_1 t + d_2 t^2 + d_3 t^3}\right) \quad \text{with} \quad t = \sqrt{\ln\left(\frac{1}{\left(1 - H(u)\right)^2}\right)} \quad \text{for}$$
$$0.5 < H(u) \le 1 \tag{9}$$

The rational approximation constants [25] are:

$$C_0 = 2.515517; C_1 = 0.802853; C_2 = 0.010328;$$
$$d_1 = 1.432788; d_2 = 0.189269; d_3 = 0.001308.$$

By construction, SPI ~ N(0, 1): positive values indicate above-average precipitation, negative values indicate deficit. The timescale k (here $k = 3$ months) determines the accumulation window: SPI-3 for May-June-July (MJJ) reflects early-season moisture availability, while SPI-3 for August-September-October (ASO) captures the core of the rainy season.

2.2.2. Standardized Precipitation Evapotranspiration Index (SPEI)

The SPEI [16] extends the SPI by incorporating the climatic water balance, making it sensitive to both precipitation deficits and thermally driven evaporative demand. It is particularly well-suited for detecting the thermal amplification of drought under climate warming [17]. The SPEI is derived from the monthly climatic water balance D_i and fitted to a three-parameter log-logistic distribution, as described below.

- **Monthly climatic water balance**

$$D_i = P_i - PET_i \tag{10}$$

where P_i is precipitation (mm) and PET_i is potential evapotranspiration (mm) for month i.

- **Temporal aggregation at timescale k**

$$D_n^k = \sum_{i=0}^{k=1} P_{n-1} - PET_{n-1} \tag{11}$$

where k is the accumulation timescale (here k = 3 months) and n the reference month.

- **Fitting the log-logistic distribution**

The D series is fitted to the three-parameter log-logistic distribution, whose PDF and CDF are:

$$f(x) = \frac{\beta}{\alpha}\left(\frac{x-\gamma}{\alpha}\right)^{\beta-1}\left[1 + \left(\frac{x-\gamma}{\alpha}\right)^{\beta-1}\right]^{-2} \tag{12}$$

$$F(x) = \left[1 + \left(\frac{\alpha}{x-y}\right)\beta\right]^{-1} \tag{13}$$

The three parameters α (scale), β (shape), and γ (location, lower bound of D) are estimated by the L-moments method [16].

- **Normal quantile transformation (SPEI value)**

The exceedance probability $p = 1 - F(x)$ is transformed into the SPEI using the same rational approximation as for the SPI:

$$\text{SPEI} = W - \frac{C_0 + C_1 W + C_2 W^2}{1 + d_1 W + d_2 W^2 + d_3 W^3}. \quad (14)$$

where $W = \sqrt{-2\ln(P)}$ for $p \le 0.5$. If $p > 0.5$, p is replaced by $1-P$ and the sign of SPEI is reversed. Constants C_0, …, d_3 are identical to those in Equations (8) - (9).

Positive SPEI values denote wetter-than-average conditions; negative values indicate water deficit. The SPI-SPEI divergence—*i.e.*, cases where SPI ≥ 0 but SPEI < 0—signals drought driven predominantly by evaporative demand rather than precipitation deficit, a signature of thermally amplified drought [16].

SPI and SPEI values were computed in Python using the *spei* package [26], which implements the gamma and log-logistic distribution fitting procedures and normal quantile transformations described in. [15] and [16], respectively.

2.2.3. Drought Classification Criteria

After computing the SPI and SPEI indices, the resulting values must be converted into discrete drought classes to allow meaningful interpretation. By conventional definition, a drought is considered to begin when the SPI/SPEI value falls below or equals −1, and it ends when the value returns to positive. Consequently, positive SPI/SPEI values indicate wet conditions, while negative values indicate dry conditions. In the present study, we adopt the classification thresholds presented in **Table 1**, which are based on the scheme proposed by [16]. This approach refines the traditional SPI/SPEI categories (e.g., [27]) by distinguishing moderately, severely, and extremely wet or dry conditions within a symmetric range of standardized index values, thereby providing a more nuanced framework for interpreting drought intensity.

Table 1. SPI/SPEI drought and wet classification thresholds [17].

SPI/SPEI threshold	Drought/wet category
SPI/SPEI > 1.83	Extremely wet
1.43 < SPI/SPEI ≤ 1.83	Severely wet
1.00 < SPI/SPEI ≤ 1.43	Moderately wet
−1.00 ≤ SPI/SPEI ≤ 1.00	Near normal
−1.43 ≤ SPI/SPEI < −1.00	Moderate drought
−1.83 ≤ SPI/SPEI < −1.43	Severe drought
SPI/SPEI < −1.83	Extreme drought

Once computed, SPI and SPEI values are classified into discrete drought or wet categories using the thresholds of [17], presented in **Table 1**. A drought episode is conventionally defined as beginning when SPI/SPEI ≤ −1.00 and ending when the index returns to positive values [15] [17]. This seven-class scheme refines the original [15] classification by explicitly distinguishing moderate, severe, and extreme conditions in both the wet and dry regimes, providing a symmetric and more nuanced framework for interpreting drought intensity.

2.3. Trend Analysis and Change Point Detection

Long-term monotonic trends in the seasonal SPI-3 and SPEI-3 series (MJJ and ASO) were assessed using the modified Mann-Kendall test proposed by [28], which corrects the original Mann-Kendall statistic for the inflation of variance caused by positive serial autocorrelation—a systematic feature of 3-month accumulation indices such as SPI-3 and SPEI-3, where successive seasonal windows overlap and are therefore not independently distributed. Applying the original Mann-Kendall test [29] [30] to autocorrelated series inflates the test statistic and increases the probability of spurious trend detection (Type I error); the Hamed-Rao correction adjusts the variance of S by a factor derived from the rank-based autocorrelation structure of the series, restoring the nominal significance level.

The Mann-Kendall statistic S is defined as:

$$S = \sum_{i=1}^{n-1} \sum_{j=i+1}^{n} \operatorname{sgn}\left(x_j - x_i\right) \tag{15}$$

where $\operatorname{sgn}(X) = 1$ if $X > 0$, 0 if $X = 0$, and -1 if $X < 0$.

The standardized test statistic Z is computed as:

$$Z = \begin{cases} \dfrac{S-1}{\sqrt{V^*(S)}} & \text{if} \quad S > 0 \\ 0 & \text{if} \quad S = 0 \\ \dfrac{S+1}{\sqrt{V^*(S)}} & \text{if} \quad S < 0 \end{cases} \tag{16}$$

where $V^*(S)$ is the autocorrelation-corrected variance of S [28]. A positive Z indicates an increasing trend and a negative Z a decreasing trend; trends are considered significant at $p < 0.05$ ($|Z| > 1.96$). The magnitude of the trend was estimated using Sen's non-parametric slope estimator [31] expressed in index units per decade:

$$\beta = \operatorname{median}\left(\frac{x_j - x_i}{j - i}\right), \forall j > i \tag{17}$$

Structural change points in the seasonal series were identified using the non-parametric Pettitt test [32], which detects a single abrupt shift in the mean of a series without requiring any assumption on the distributional form. The Pettitt statistic is:

$$K_T = \max_{1 \le t \le n} \left|U_{t,n}\right|, U_{t,n} = \sum_{i=1}^{t} \sum_{j=t+1}^{n} \operatorname{sgn}\left(x_i - x_j\right) \tag{18}$$

The approximate probability of a significant change point is given by

$$P \approx 2\exp\left(-6KT^2 \middle/ \left(n^3 + n^2\right)\right) \tag{19}$$

Change points with $p < 0.05$ are reported as significant.

All tests were implemented in Python using the pymannkendall [33] and pyhomogeneity packages on annual MJJ and ASO index values. For a comprehensive treatment of these methods in hydroclimatological applications, the reader is referred to [34] and [35].

3. Results and Discussions

3.1. Monthly Drought Dynamics: SPI-3 and SPEI-3 Temporal Evolution (1981-2021)

The monthly time series of SPI-3 and SPEI-3 show in **Figure 2** provide a continuous view of drought onset, duration, and cessation at each of the nine synoptic stations across the three climatic zones of Burkina Faso. Three agronomically relevant features emerge from this temporal perspective.

Across all zones, the early period (1981-1990) is marked by sustained sequences of negative anomalies frequently breaching the severe (≤−1.43) and extreme (≤−1.83) drought thresholds, with the Sahelian stations (Ouahigouya, Dori) and the Sudano-Sahelian stations (Dédougou, Fada Ngourma) displaying the longest consecutive dry spells. The SPEI-3 signal is generally more intense than SPI-3 during this phase at Dori and Boromo, indicating that elevated evaporative demand compounded rainfall deficits even during the most drought-affected decade. From 1991 onward, both indices shift predominantly toward near-normal to positive values, reflecting the partial rainfall recovery documented across the Sahel, though isolated threshold-crossing events persist at all stations. After 2000, episodes where SPEI-3 crosses the severe drought threshold while SPI-3 remains near-normal become increasingly visible, particularly in the Sudano-Sahelian zone (Ouagadougou, Dédougou), confirming a growing decoupling between precipitation deficits and evapotranspiration-driven water stress with direct consequences for rainfed agriculture. The post-2015 period is further characterized by a marked increase in the frequency and amplitude of threshold-crossing events in both directions at all stations, consistent with the intensification of interannual hydroclimatic variability discussed in Section below.

To complement this monthly perspective and identify the dominant drought years at the seasonal scale, we next examine SPI-3 and SPEI-3 drought categories aggregated over the early rainy season (MJJ: May-June-July) and the late rainy season (ASO: August-September-October).

3.2. Seasonal Drought Variability during the Early and Late Rainy Season (1981-2021)

Figure 3 presents the spatio-temporal variability of SPI-3 and SPEI-3 drought categories at nine synoptic stations in Burkina Faso for the early rainy season (MJJ: May-June-July) and the late rainy season (ASO: August-September-October) over the period 1981-2021. Stations are grouped according to the three climatic zones delineated by the 600 and 900 mm/year mean annual rainfall isohyets (**Figure 1**): the Sahelian zone (Ouahigouya, Dori), the Sudano-Sahelian zone (Ouagadougou, Dédougou, Boromo, Fada Ngourma), and the Sudanian zone (Bobo-Dioulasso, Gaoua, Pô). Three distinct temporal phases emerge from the heatmaps, each reflecting a different interplay between rainfall variability, evaporative demand, and climatic zone.

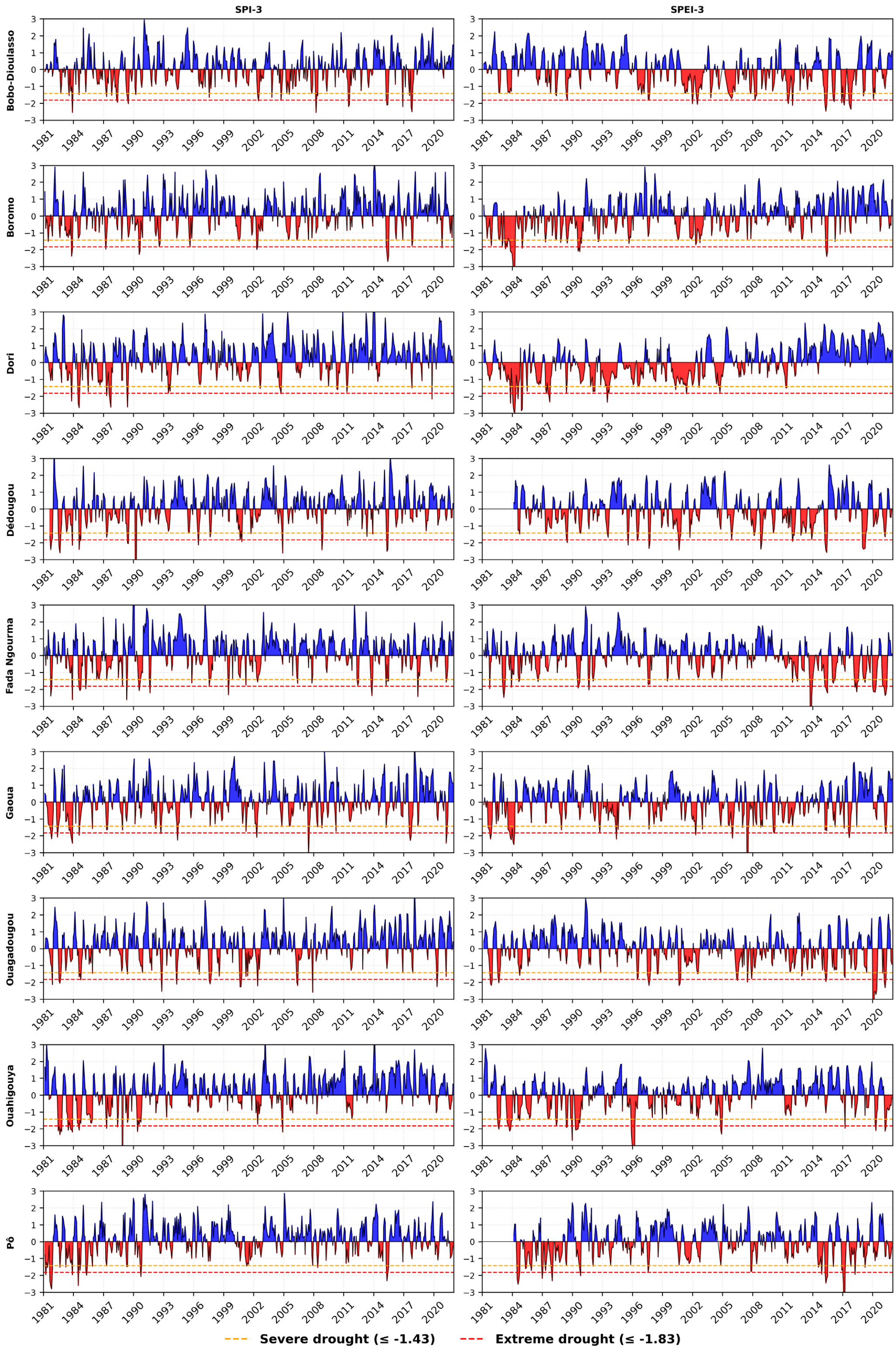

Figure 2. Monthly time series of SPI-3 (left panels) and SPEI-3 (right panels) at nine synoptic stations in Burkina Faso over the period 1981-2021. Positive values (blue) indicate wetter-than-normal conditions; negative values (red) indicate drier-than-normal conditions. Dashed lines mark the severe drought threshold (SPI-3/SPEI-3 ≤ −1.5, orange) and the extreme drought threshold (SPI-3/SPEI-3 ≤ −2.0, red), following the classification of [15].

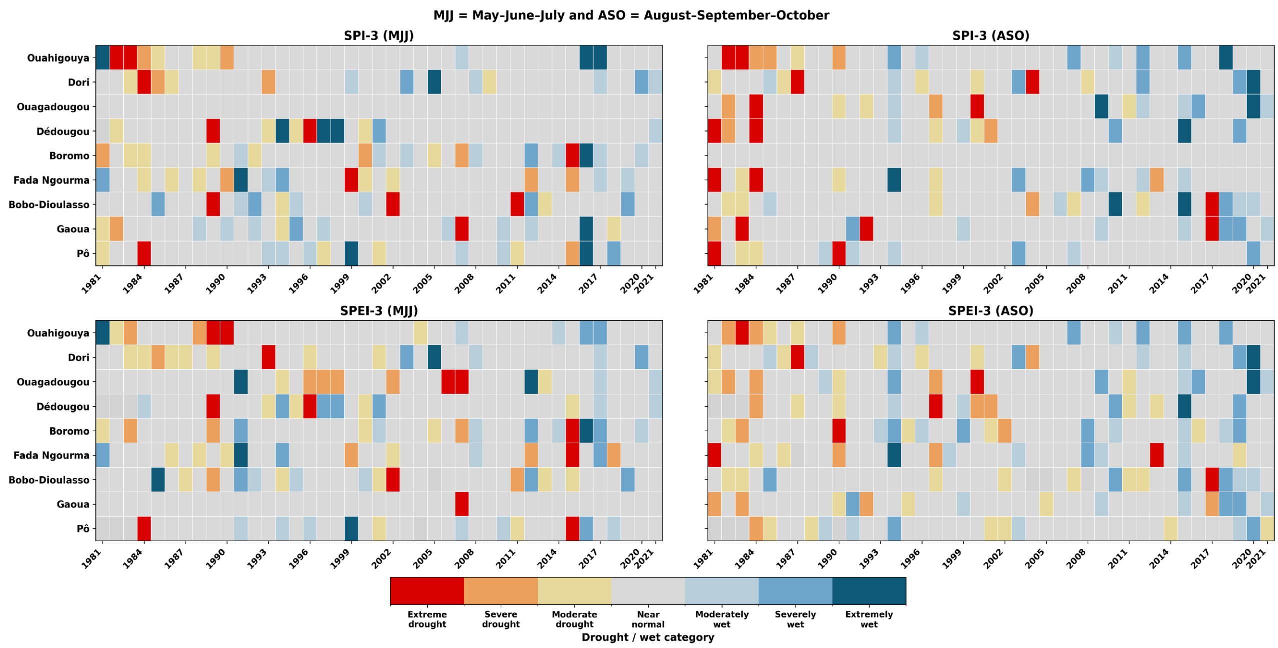

Figure 3. Spatio-temporal variability of meteorological drought at nine synoptic stations in Burkina Faso (1981-2021): SPI-3 and SPEI-3 drought categories for the early rainy season (MJJ: May-June-July) and the late rainy season (ASO: August-September-October).

3.2.1. Early Period (1981-1990): Widespread Drought Dominance with a Northward Amplification

The first decade is characterized by a marked concentration of severe and extreme drought events across all three climatic zones, with the most persistent and intense signal observed in the Sahelian zone. Ouahigouya recorded extreme drought conditions in both MJJ (SPI-3 = −2.11 in 1982; −2.08 in 1983) and ASO (SPI-3 = −1.99 in 1982; −2.05 in 1983), while Dori exhibited extreme drought in MJJ 1984 (SPI-3 = −2.42) and a severe drought in ASO 1987 (SPI-3 = −2.65). These values reflect the persistence of the pan-Sahelian dry anomaly documented across West Africa during this period [36]. In the Sudano-Sahelian zone, Fada Ngourma recorded extreme drought in MJJ 1990 and in ASO 1981 (SPI-3 = −2.40), and Dédougou in MJJ 1989 (SPI-3 = −2.06) and ASO 1981 (SPI-3 = −2.41) and 1984 (SPI-3 = −1.87). The Sudanian zone was not exempt: Pô experienced extreme drought in ASO 1981 (SPI-3 = −2.65) and Bobo-Dioulasso in MJJ 1989 (SPI-3 = −2.03), indicating that this early drought episode was spatially coherent across the entire national territory. Crucially, SPI-3 and SPEI-3 signals are broadly consistent during this phase, confirming that the drought was primarily driven by rainfall deficits rather than by elevated evaporative demand, regardless of climatic zone.

3.2.2. Transitional Period (1991-2010): Attenuation, Partial Recovery, and Emerging Zone-Specific Divergences

Following 1990, the heatmaps show a widespread shift toward near-normal conditions across all zones and both seasons, consistent with the documented partial recovery of Sahelian rainfall referred to as the "Sahel greening" [37]. In the Sahelian zone, isolated but marked positive anomalies re-emerge, most notably at Dori in MJJ 2005 (SPI-3 = +2.26, extremely wet), signaling the return of episodic intense rainfall events. In the Sudano-Sahelian zone, Fada Ngourma recorded an extremely wet ASO in 1994 (SPI-3 = +2.33), while Boromo presents a strikingly uniform near-normal signal throughout ASO for the entire study period, likely reflecting its central geographic position and exposure to a broader range of mesoscale convective systems that tend to dampen seasonal extremes. In the Sudanian zone, conditions remained predominantly near-normal during this phase, with occasional moderately wet years at Gaoua and Pô. However, this transitional period reveals an important zone-specific divergence between SPI-3 and SPEI-3: in the Sudano-Sahelian zone, SPEI-3 flags severe drought conditions at Ouagadougou in MJJ 1996-1998 and extreme drought in MJJ 2006-2007, while SPI-3 remains near-normal for the same years. Similarly, Dédougou shows severe drought in SPEI-3 for MJJ 1996 and 2015 where SPI-3 is near-normal. These discrepancies indicate that rainfall amounts were not markedly deficient during these episodes, but that increased evapotranspiration demand—consistent with rising temperatures in the Sudano-Sahelian belt—amplified the hydrological stress beyond what precipitation alone would suggest. This finding underlines the added diagnostic value of the SPEI over the SPI under warming conditions, as previously noted by [16].

3.2.3. Recent Period (2015-2021): Intensification of Extremes and Increased Cross-Zone Synchronicity

The most recent years reveal a notable increase in interannual variability amplitude across all three climatic zones, with extreme events of both signs occurring in close succession and often simultaneously across zones. On the wet side, 2016 stands out as an exceptional year: extremely wet conditions were simultaneously recorded in the Sahelian zone (Ouahigouya, SPI-3 MJJ = +2.06), the Sudano-Sahelian zone (Boromo, SPI-3 MJJ = +2.12), and the Sudanian zone (Gaoua, SPI-3 MJJ = +2.11; Pô, SPI-3 MJJ = +1.87), indicating a country-wide pluviometric surplus. In ASO, this synchronicity is equally visible in 2020, with extremely wet conditions recorded at Dori (Sahelian, SPI-3 = +2.47) and Ouagadougou (Sudano-Sahelian, SPI-3 = +1.85). On the dry side, contrasting signals emerge: Bobo-Dioulasso (Sudanian zone) experienced extreme drought in ASO 2017 under both indices (SPI-3 = −2.24; SPEI-3 = −2.23), while Fada Ngourma (Sudano-Sahelian) recorded extreme drought under SPEI-3 MJJ 2015 (−2.22) with SPI-3 near-normal, again pointing to an evapotranspiration-driven drought component in the central zone. This alternation between severe dry and wet extremes within short time windows across all zones is consistent with the intensification of rainfall variability projected under climate change scenarios for the West African Sahel [37], and represents a critical challenge for water resource management and agricultural planning in Burkina Faso.

3.2.4. North-South Gradient and Index Consistency

Considered over the full period and both seasons, the three climatic zones exhibit a coherent latitudinal gradient in drought severity: the Sahelian zone is most frequently and most intensely affected during the early period, the Sudano-Sahelian zone shows the strongest SPI-3/SPEI-3 divergence during the transitional period, and the Sudanian zone, while less drought-prone overall, participates in the cross-zone synchronicity of recent extreme events. SPI-3 and SPEI-3 produce broadly comparable drought classifications throughout, reinforcing diagnostic reliability. Where discrepancies occur, they are systematically oriented toward more intense drought classification by SPEI-3, particularly in the Sudano-Sahelian zone after 2000, supporting the hypothesis of an increasing evaporative contribution to drought severity under ongoing warming. One outlier value of SPEI-3 MJJ = −7.87 at Gaoua (Sudanian zone) in 2007 is physically implausible and likely results from a missing or erroneous PET value in the source data; this data point must be verified and masked prior to final figure production.

3.3. Drought Frequency and Mean Duration by Intensity Class

The spatial contrasts in drought frequency and mean duration across intensity classes and climatic zones, as detected by both SPI-3 and SPEI-3, are synthesized in Figure 4.

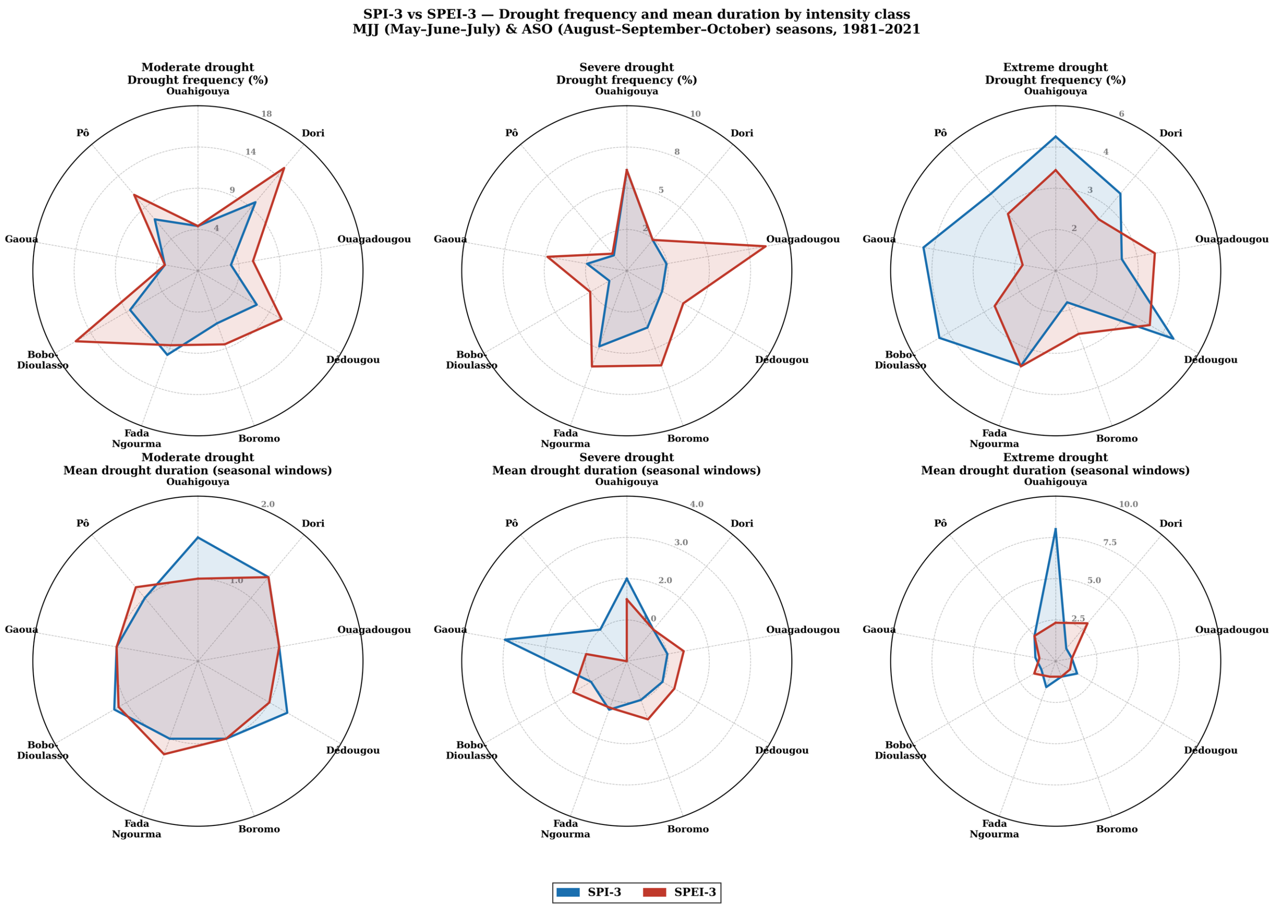

Figure 4. Radar charts of SPI-3 and SPEI-3 drought frequency (%, upper panels) and mean drought duration (seasonal windows, lower panels) by intensity class at nine synoptic stations in Burkina Faso over the period 1981-2021. Each axis represents one station; values are computed over the early (MJJ: May-June-July) and late (ASO: August-September-October) rainy season windows.

Figure 4 reveals contrasting detection patterns between SPI-3 and SPEI-3 across the three climatic zones, both in terms of frequency and episode duration.

SPEI-3 systematically detects higher moderate and severe drought frequencies than SPI-3 across all zones, with the divergence most pronounced in the Sudano-Sahelian zone (Ouagadougou, Dédougou, Fada Ngourma) and, to a lesser extent, in the Sahelian zone (Dori). This pattern is scientifically consistent and well-documented in the literature. [16] demonstrated that the SPEI, by incorporating the evaporative demand through the P-PET balance, captures atmospheric water stress that is invisible to precipitation-only indices such as the SPI. Under the sustained warming observed in West Africa since the 1990s [38], potential evapotranspiration has increased independently of rainfall, generating moderate-to-severe hydric stress even during years of near-normal precipitation. This mechanism is particularly active in the Sudano-Sahelian zone, where temperature anomalies are amplified relative to the wetter Sudanian south [39]. The higher SPEI-3 frequencies in these two classes are therefore not a statistical artefact but a physically grounded signal of evapotranspiration-driven agricultural drought.

The pattern reverses for extreme drought: SPI-3 detects higher frequencies than SPEI-3, most visibly at Pô, Bobo-Dioulasso, and Ouahigouya. This is also consistent with known index behavior. Extreme drought events (index < -1.83) are typically associated with catastrophic rainfall deficits—as observed during 1982-1984 across the Sahel—where precipitation collapse so severe that the additional evaporative signal of SPEI becomes secondary relative to the raw precipitation anomaly captured by SPI. Under such conditions, the SPI responds more sharply because the gamma distribution fitted to precipitation is more sensitive to deep left-tail events than the log-logistic distribution fitted to the P-PET balance, which integrates a smoother combined signal [40]. This explains why SPI-3 leads in the extreme class while SPEI-3 leads in moderate and severe classes.

The duration panels reveal a complementary contrast. SPI-3 produces longer mean episode durations for extreme drought, driven by the sustained multi-window Sahelian drought of 19821990 visible as the spike at Ouahigouya (~8 seasonal windows). SPEI-3, by contrast, generates longer durations for moderate and severe classes, particularly in the Sudano-Sahelian zone, reflecting the chronic low-intensity water stress driven by rising PET that persists across multiple consecutive seasonal windows even when rainfall partially recovers. This distinction carries direct agronomic implications: SPI-3 better captures acute, catastrophic drought episodes damaging to annual crop establishment, while SPEI-3 better characterizes the chronic, cumulative water stress that progressively degrades soil moisture reserves and reduces agricultural yields over successive seasons—a process of particular concern for the smallholder farming systems of Burkina Faso [41].

In semi-arid Sahelian environments such as Burkina Faso, where rainfall variability remains the primary driver of drought but rising temperatures increasingly amplify evaporative demand, SPEI-3 is the more comprehensive and agronomically relevant indicator for frequency assessment, as it captures both precipitation deficits and evapotranspiration-driven stress that SPI-3 systematically misses, particularly for moderate and severe classes; however, SPI-3 remains the more reliable indicator for detecting extreme drought episodes, whose intensity and duration are overwhelmingly controlled by catastrophic rainfall deficits that render the evaporative component secondary—a complementarity that justifies the joint use of both indices rather than the exclusive adoption of either one.

3.4. Intra-Seasonal and Inter-Index Contrasts in Drought Occurrence across Climatic Zones

The seasonal distribution of drought occurrence across intensity classes and climatic zones, as detected by SPI-3 and SPEI-3, is examined in Figure 5. It reveals marked asymmetries between MJJ and ASO drought occurrence, between SPI-3 and SPEI-3, and across the three climatic zones, with patterns that are both scientifically coherent and agronomically significant.

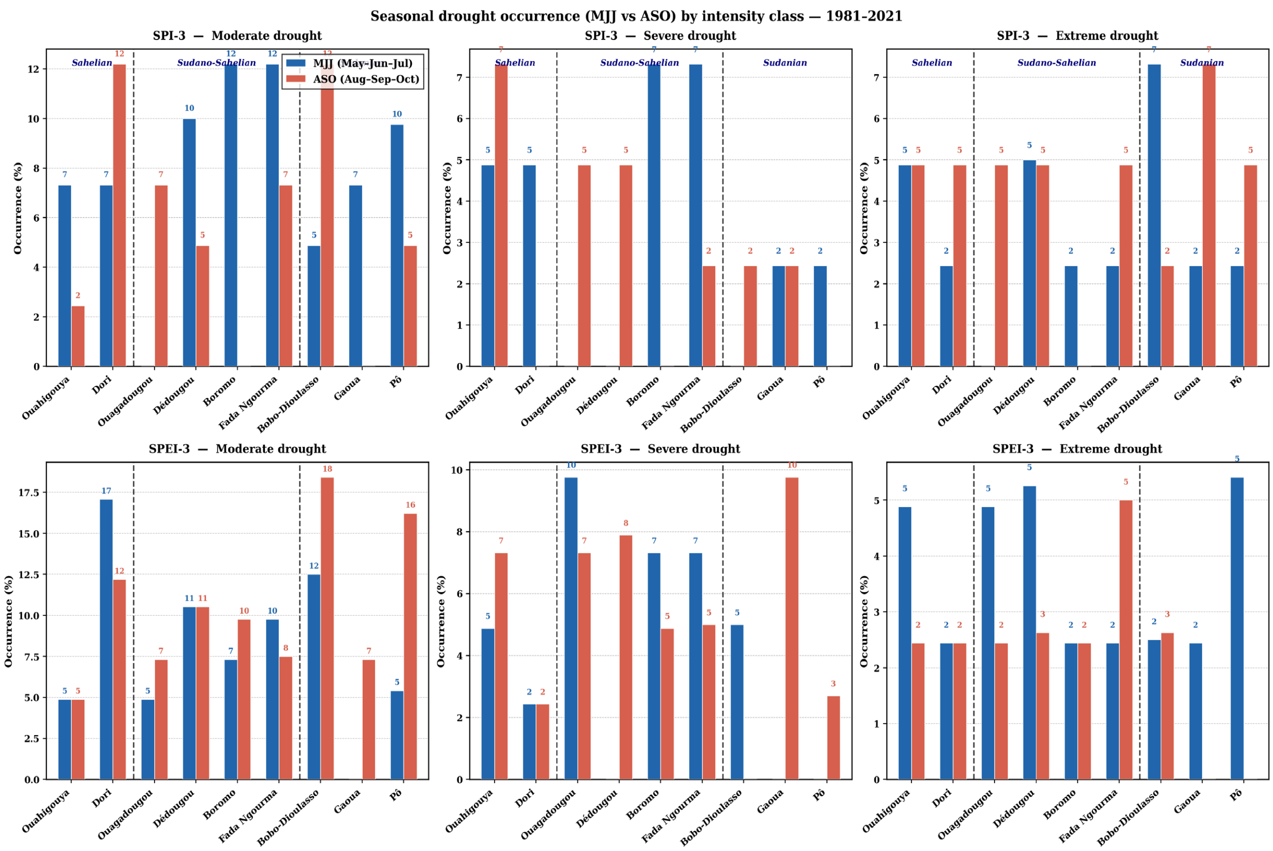

Figure 5. Seasonal drought occurrence (%) by intensity class at nine synoptic stations in Burkina Faso (1981-2021), comparing the early rainy season (MJJ: May-June-July, blue bars) and the late rainy season (ASO: August-September-October, red bars) for SPI-3 (upper panels) and SPEI-3 (lower panels). Occurrence is computed as the percentage of seasonal windows classified as Moderate ($-1.43 \le$ index < -1.00), Severe ($-1.83 \le$ index < -1.43), or Extreme (index < -1.83) drought out of 41 available observations per season and per station. Dashed vertical lines delimit the three climatic zones: Sahelian (Ouahigouya, Dori), Sudano-Sahelian (Ouagadougou, Dédougou, Boromo, Fada Ngourma), and Sudanian (Bobo-Dioulasso, Gaoua, Pô). Values above bars indicate occurrence in percent.

MJJ dominance across all zones. Under SPI-3, moderate drought occurrence is systematically higher in MJJ than in ASO across the three climatic zones, with the most pronounced contrast observed in the Sudano-Sahelian zone: Boromo (12% MJJ vs 7% ASO), Fada Ngourma (12% MJJ vs 7% ASO), and Dédougou (10% MJJ vs 5% ASO). This MJJ dominance reflects the higher interannual variability of rainfall onset over Burkina Faso, where delayed or insufficient early-season rains—a recurrent feature of the West African monsoon—generate moderate water deficits that normalize by the peak of the rainy season [42]. In the Sahelian zone, Dori shows the inverse pattern (5% MJJ vs 12% ASO under SPI-3), suggesting that in the northernmost station the late-season rainfall, which is already structurally limited, is more prone to deficits than the early season.

SPEI-3 dramatically amplifies moderate drought occurrence relative to SPI-3 across all zones, confirming the evapotranspiration-driven component discussed in previous Section. The Sudano-Sahelian zone reaches 17% - 18% at Dori and Bobo-Dioulasso respectively, and the Sudanian zone shows a striking ASO dominance at Pô (5% MJJ vs 16% ASO) and Bobo-Dioulasso (13% MJJ vs 18% ASO). This ASO reversal in the Sudanian zone under SPEI-3 is physically interpretable: by August-October, the accumulated thermal energy of the rainy season drives PET to its seasonal peak, amplifying the atmospheric water demand and generating SPEI deficits even when precipitation remains adequate by SPI standards. This mechanism is consistent with findings by [43] for tropical semi-humid regions under warming conditions.

Sahelian and Sudano-Sahelian concentration in MJJ. Severe drought under SPI-3 is predominantly a MJJ phenomenon in the Sahelian (Ouahigouya 5%, Dori 5%) and Sudano-Sahelian zones (Ouagadougou 5%, Dédougou 5%, Boromo 5%), with near-zero ASO occurrence except at Dori (7% ASO). Under SPEI-3, severe drought occurrence increases substantially, particularly in ASO for the Sudano-Sahelian zone (Ouagadougou 7%, Dédougou 8%, Fada Ngourma 7%) and for the Sudanian zone at Pô (10% ASO vs 5% MJJ), again reflecting the late-season evaporative amplification.

For the extreme class, SPI-3 and SPEI-3 produce broadly similar occurrence values (2% - 5% range), with no systematic seasonal asymmetry across zones. This convergence is consistent with the index behavior discussed in Section 3.3: extreme drought episodes are driven by catastrophic precipitation deficits that override the differential evaporative signal, making SPI-3 and SPEI-3 equivalent detectors. The slight SPI-3 lead at Bobo-Dioulasso in MJJ (7%) and the SPEI-3 lead at Pô in ASO (5%) are the only notable exceptions, likely reflecting localized precipitation-PET interactions.

Across all intensity classes, the MJJ season is the primary locus of drought occurrence under SPI-3, reflecting the sensitivity of rainfall onset to interannual variability. SPEI-3 redistributes and amplifies this signal toward ASO, particularly in the Sudanian zone, where late-season evaporative demand is highest. This seasonal asymmetry has direct implications for agricultural drought risk assessment:

early-season SPI-3 deficits threaten crop establishment and germination, while late-season SPEI-3 deficits threaten grain filling and yield consolidation—two distinct vulnerability windows that require differentiated monitoring strategies [41].

3.5. Historical Drought Trend Analysis and Change Point Detection (1981-2021)

3.5.1. Long-Term Drought Trends: Mann-Kendall Test and Sen's Slope

The spatial and temporal patterns of SPI-3 and SPEI-3 trends across the nine synoptic stations are illustrated in Figure 6 and Figure 7. Results from the Hamed-Rao modified Mann-Kendall test [29] reveal a predominantly positive trend in both indices over 1981-2021, indicating a general shift toward wetter seasonal conditions consistent with the post-1990s Sahelian rainfall recovery documented in the literature [36] [44]. However, the spatial coherence, seasonal asymmetry, and index-specific nature of these trends vary markedly across climatic zones.

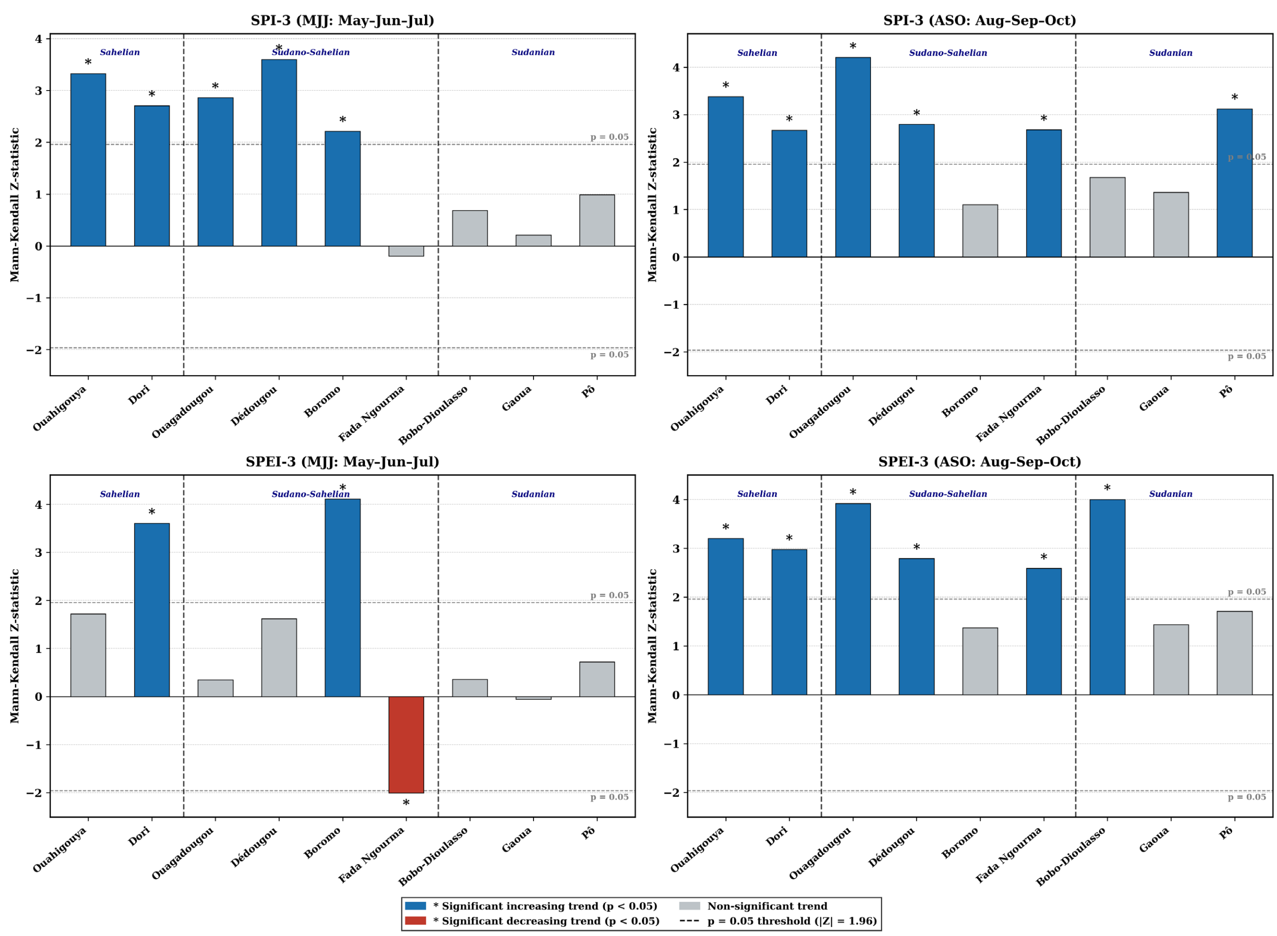

Figure 6. Mann-Kendall Z-statistics for SPI-3 and SPEI-3 seasonal drought trends at nine synoptic stations in Burkina Faso (1981-2021), for the early rainy season (MJJ: May-June-July, upper panels) and the late rainy season (ASO: August-September-October, lower panels). Blue bars indicate significant increasing trends ($p < 0.05$), red bars significant decreasing trends ($p < 0.05$), and grey bars non-significant trends. The dashed horizontal lines mark the $p = 0.05$ significance threshold ($|Z| = 1.96$). Asterisks (*) denote statistical significance. Dashed vertical lines delimit the three climatic zones: Sahelian (Ouahigouya, Dori), Sudano-Sahelian (Ouagadougou, Dédougou, Boromo, Fada Ngourma), and Sudanian (Bobo-Dioulasso, Gaoua, Pô).

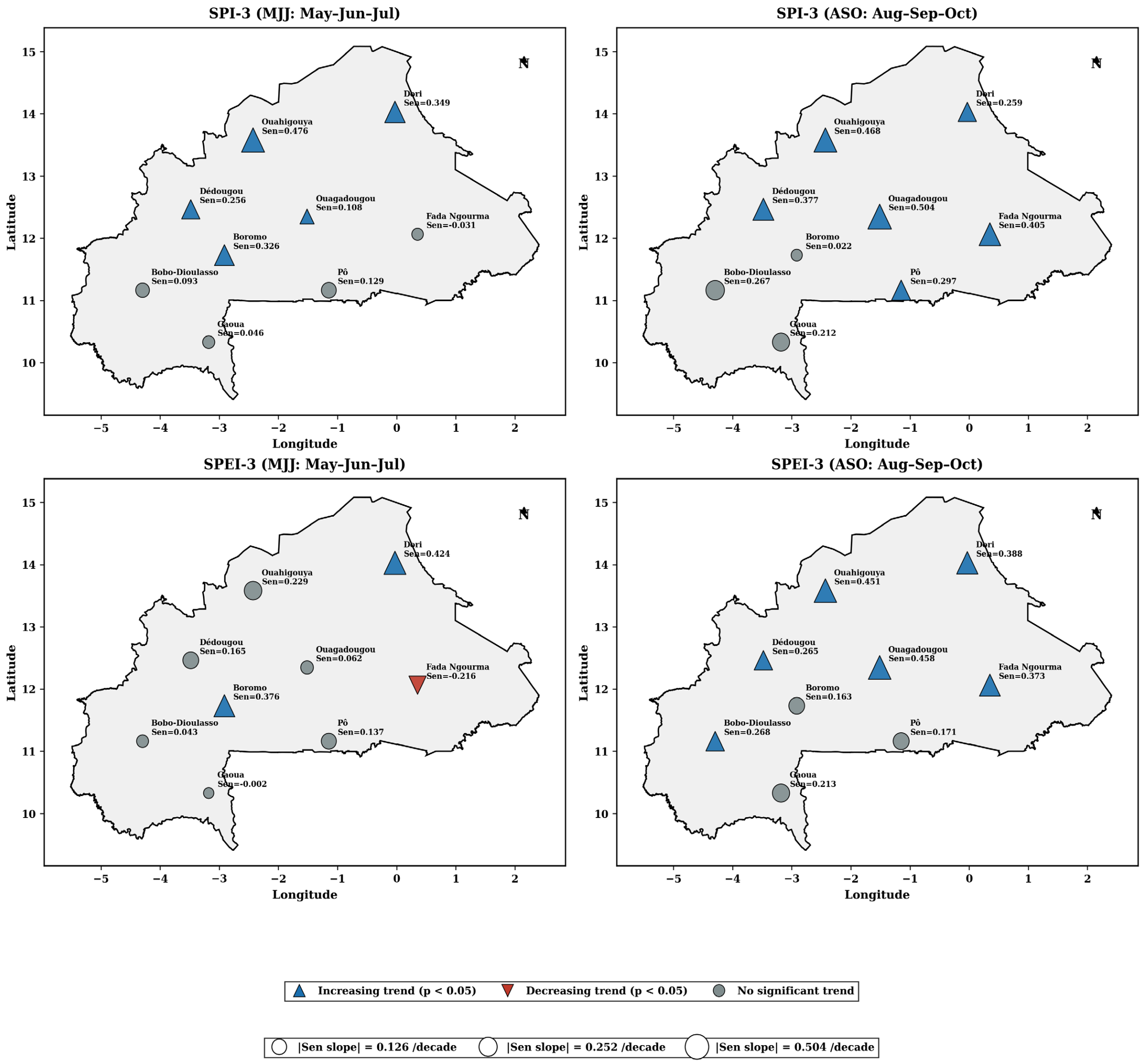

Figure 7. Spatial distribution of SPI-3 and SPEI-3 seasonal drought trends at nine synoptic stations in Burkina Faso (1981-2021). Blue upward triangles indicate significant increasing trends ($p < 0.05$); red downward triangles indicate significant decreasing trends ($p < 0.05$); grey circles indicate non-significant trends. Symbol size is proportional to the absolute value of Sen's slope magnitude (units per decade). Values next to each station indicate Sen's slope [32].

For Sahelian zone (Ouahigouya and Dori), both stations exhibit significant positive SPI-3 trends in both seasons. For MJJ, Ouahigouya shows the strongest signal ($Z = 3.325$, $p = 0.0009$, Sen's slope = +0.476/decade) followed by Dori ($Z = 2.707$, $p = 0.007$, slope = +0.349/decade). In ASO, the trends remain highly significant and of comparable magnitude (Ouahigouya: $Z = 3.381$, $p = 0.0007$, slope = +0.468/decade; Dori: $Z = 2.670$, $p = 0.008$, slope = +0.259/decade). Under SPEI-3, Dori retains a significant positive trend in both MJJ ($Z = 3.605$, $p = 0.0003$, slope = +0.424/decade) and ASO ($Z = 2.976$, $p = 0.003$, slope = +0.388/decade), while Ouahigouya's SPEI-3 MJJ trend, though positive, does not reach significance ($Z = 1.718$, p =

0.086), suggesting that the rainfall recovery at this station during the early season is partially offset by an increasing evaporative demand that moderates the net hydric balance improvement. Both stations show significant positive SPEI-3 trends in ASO (Ouahigouya: $Z = 3.201$, p = 0.001; Dori: $Z = 2.976$, p = 0.003), confirming a robust late-season recovery across the Sahelian zone.

In the Sudano-Sahelian zone, trends vary spatially and display a pronounced seasonal asymmetry. This zone exhibits the most complex trend structure. Under SPI-3 in MJJ, Ouagadougou ($Z = 2.860$, p = 0.004, slope = +0.108/decade), Dédougou ($Z = 3.597$, p = 0.0003, slope = +0.256/decade), and Boromo ($Z = 2.213$, p = 0.027, slope = +0.326/decade) show significant positive trends, while Fada N'Gourma stands out as the only station with a near-zero and non-significant trend ($Z = -0.194$, p = 0.846, slope = −0.031/decade). In ASO under SPI-3, the trend field reorganizes: Ouagadougou becomes the strongest signal in the entire dataset ($Z = 4.208$, $p < 0.0001$, slope = +0.504/decade), Fada Ngourma recovers a significant positive trend ($Z = 2.684$, p = 0.007, slope = +0.405/decade), while Boromo loses significance ($Z = 1.101$, p = 0.271), suggesting that the rainfall recovery in the western Sudano-Sahelian sector is concentrated in the late season rather than at monsoon onset.

Under SPEI-3, the contrast between MJJ and ASO sharpens further. In MJJ, only Boromo retains a significant positive SPEI-3 trend ($Z = 4.112$, $p < 0.0001$, slope = +0.376/decade), while Fada Ngourma registers the only significant decreasing trend in the entire dataset ($Z = -2.005$, p = 0.045, slope = −0.216/decade). This isolated negative SPEI-3 MJJ signal at Fada Ngourma, absent in SPI-3, indicates that at this station early-season moisture stress is increasing due to rising evapotranspiration demand even as precipitation trends remain neutral—a pattern consistent with the thermal amplification observed in the eastern Sudano-Sahelian belt under ongoing warming [38]. In SPEI-3 ASO, Ouagadougou ($Z = 3.916$, p = 0.0001), Dori ($Z = 2.976$), Dédougou ($Z = 2.791$, p = 0.005), and Fada Ngourma (Z = 2.587, p = 0.010) all show significant positive trends, underscoring that late-season hydric conditions have improved across the zone despite the early-season SPEI-3 anomaly at Fada Ngourma.

Within the Sudanian zone, MJJ trends remain largely absent while ASO signals begin to emerge. The three southern stations (Bobo-Dioulasso, Gaoua, Pô) show no significant SPI-3 or SPEI-3 trend in MJJ under any index, with Z-statistics well below the ±1.96 threshold. This absence of trend at monsoon onset in the Sudanian zone contrasts sharply with the Sahelian and Sudano-Sahelian zones and may reflect the greater stability of early-season rainfall in the humid south, where interannual variability is lower and monsoon onset is less sensitive to large-scale circulation anomalies [42]. In ASO, Pô shows a significant positive SPI-3 trend ($Z = 3.125$, p = 0.002, slope = +0.298/decade), and Bobo-Dioulasso a strong positive SPEI-3 ASO trend ($Z = 4.001$, p = 0.0001, slope = +0.268/decade) without reaching significance under SPI-3 ($Z = 1.674$, p = 0.094)—again pointing to an evapotranspiration-mediated improvement in late-season water balance in the Sudanian zone that SPI-3 alone would underdetect.

3.5.2. Structural Change Point Analysis: Pettitt Test

Figure 8 presents the results of the Pettitt test applied to drought indices over the study period, revealing two distinct temporal clusters of significant change points, the annual time series with annotated change points and pre/post-rupture means for all significant cases are provided in Supplementary **Figure S1**.

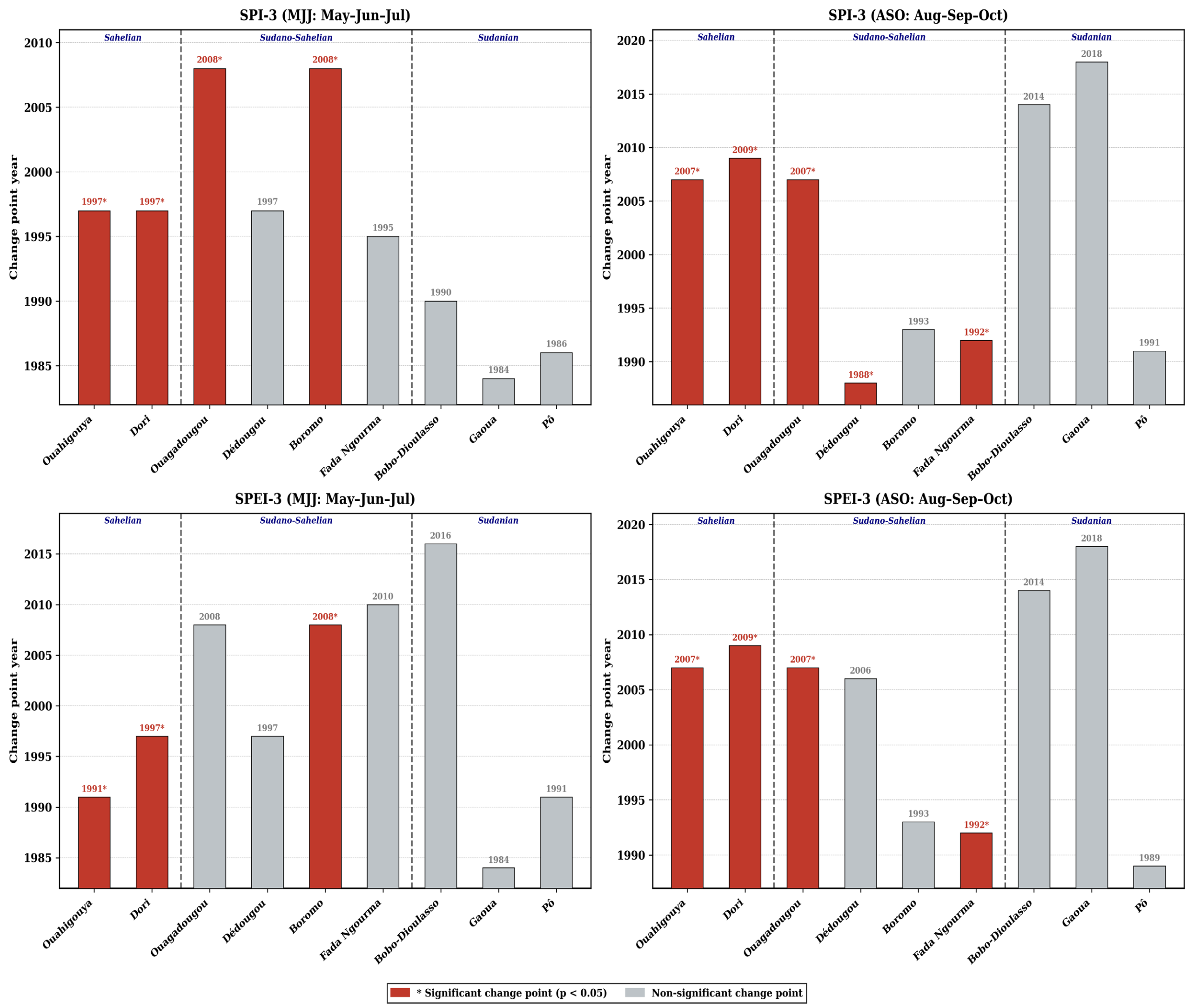

Figure 8. Pettitt test change point years for SPI-3 and SPEI-3 seasonal drought series at nine synoptic stations in Burkina Faso (1981-2021), for the early rainy season (MJJ, upper panels) and the late rainy season (ASO, lower panels). Red bars indicate statistically significant change points ($p < 0.05$); grey bars indicate non-significant change points. Asterisks (*) denote significance at $p < 0.05$. Dashed vertical lines delimit the three climatic zones. Values above bars indicate the detected change point year.

- First cluster: 1988-1997 (early recovery phase). Significant change points during this window are concentrated in the Sahelian and Sudano-Sahelian zones in MJJ under SPI-3: Ouahigouya (1997, $p = 0.004$) and Dori (1997, $p = 0.019$) both record a structural upward shift in early-season SPI-3 around 1997, consistent with the abrupt intensification of the Sahelian rainfall recovery documented after the mid-1990s [44]. Dédougou also shows a 1997 change point in SPI-3 MJJ, though not significant (p = 0.178), and Fada Ngourma records an early non-significant change point in 1992 for SPI-3 ASO (p = 0.013, significant), suggesting that the late-season recovery in the eastern Sudano-Sahelian sector preceded the early-season shift. Dédougou's SPI-3 ASO change point occurs earlier, in 1988 (p = 0.035, significant), which may be related to local rainfall redistribution rather than a basin-wide signal. Under SPEI-3, Dori's change point in MJJ (1997, p = 0.002) and Ouahigouya's ASO change point (2007, p = 0.002) confirm that the recovery signal propagated progressively from precipitation to the integrated hydric balance index.

- Second cluster: 2007-2009 (intensification phase). A second cluster of significant change points emerges in the 2007-2009 window, primarily in SPI-3 and SPEI-3 ASO for the Sahelian and Sudano-Sahelian zones. Ouahigouya (SPI-3 ASO, 2007, p = 0.003), Ouagadougou (SPI-3 ASO, 2007, p = 0.005; SPEI-3 ASO, 2007, p = 0.013), and Fada Ngourma (SPEI-3 ASO, 1992, p = 0.031) all record significant shifts, suggesting a second intensification of positive conditions after 2007 that reinforced the earlier recovery. This double-phase structure—initial shift in the mid-1990s followed by a reinforcement around 2007-2009—is consistent with the non-monotonic nature of Sahelian rainfall recovery described by [45], who documented increasing rainfall intensity and frequency of extreme wet events in the 2000s.

The Sudanian zone shows no significant Pettitt change points under any index or season, reinforcing the interpretation that long-term hydroclimatic reorganization over 1981-2021 is primarily a Sahelian and Sudano-Sahelian phenomenon, with the Sudanian zone remaining structurally stable throughout the period despite the isolated emerging ASO trends noted above.

The synthetic heatmap (**Figure 9**) consolidates the Mann-Kendall Z-statistics, Sen's slopes, and Pettitt change point years for all index-season combinations across the nine stations, providing a direct cross-reading of trend significance, magnitude, and structural timing. Several patterns stand out clearly. The upper panels confirm the northward concentration of significant positive trends, with the Sahelian zone showing the highest Z-values and largest Sen's slopes in both MJJ and ASO under SPI-3, while the Sudanian zone remains predominantly grey (non-significant). The single red cell at Fada Ngourma under SPEI-3 MJJ—the only negative significant trend in the dataset—is immediately identifiable against the otherwise positive background of the Sudano-Sahelian zone, highlighting its anomalous character. The lower panels reveal that significant Pettitt change points (dark cells) cluster in the 1997-2009 window for the Sahelian and Sudano-Sahelian zones, with a notable absence of significant structural breaks across the entire Sudanian zone, reinforcing the interpretation of a geographically bounded hydroclimatic reorganization that has not yet propagated to the southern sector of Burkina Faso.

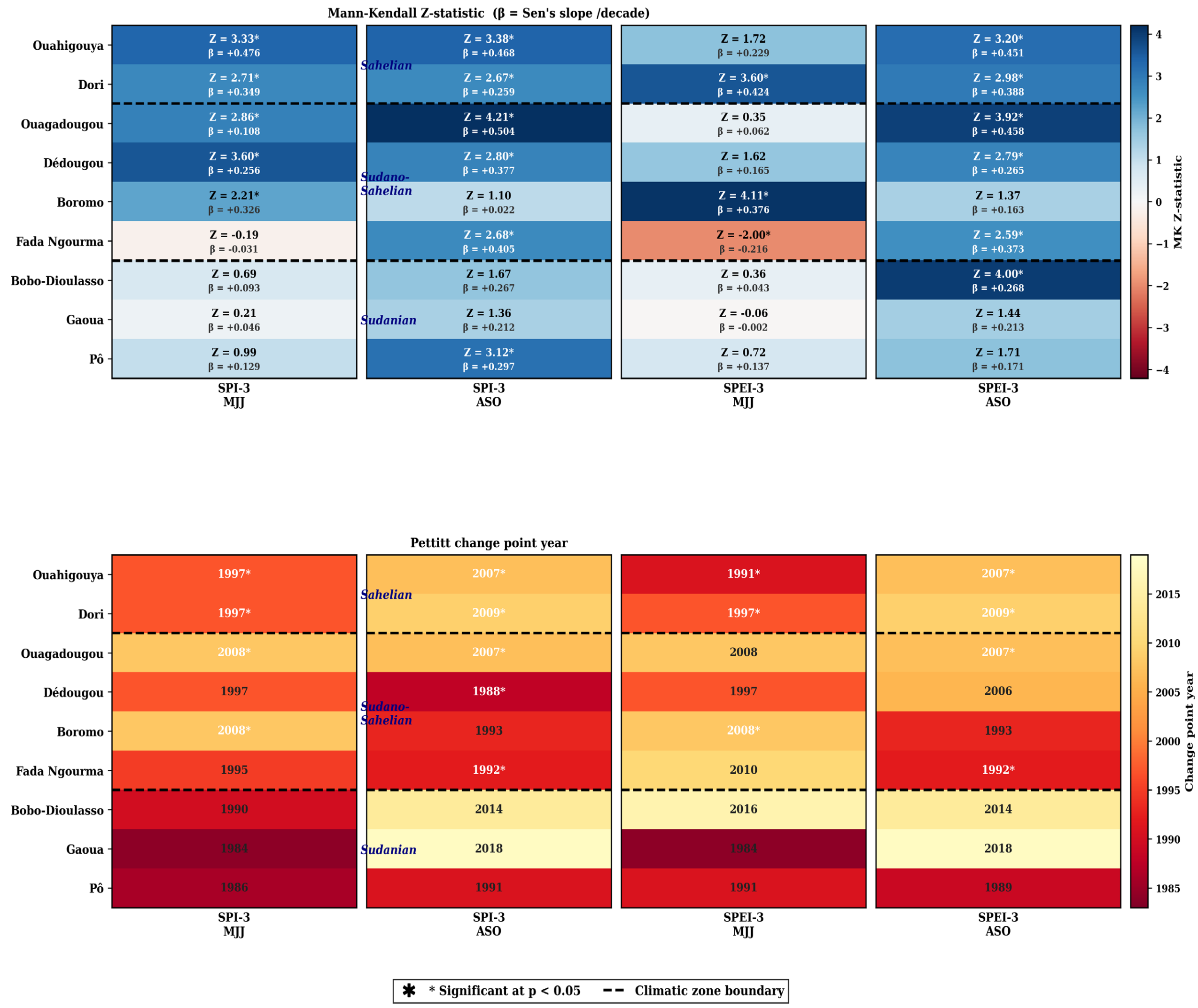

Figure 9. Synthetic heatmap of Mann-Kendall trend statistics and Pettitt change point years for SPI-3 and SPEI-3 seasonal drought series at nine synoptic stations in Burkina Faso (1981-2021). Upper panels display the Mann-Kendall Z-statistic (Hamed-Rao modified test) and Sen's slope β (units per decade) for each station-index-season combination. Lower panels display the Pettitt test change point year for each combination, with the yellow-to-dark colormap indicating earlier (darker) to later (lighter) change points. Asterisks (*) denote statistical significance at $p < 0.05$ for both the Mann-Kendall trend test and the Pettitt change point test. Dashed horizontal lines delimit the three climatic zones.

3.6. Limitations of Spatial Representativeness

Given the extreme spatial heterogeneity of mesoscale convective systems that drive Sahelian rainfall, the nine synoptic stations used in this study cannot be assumed to provide a spatially continuous or exhaustive characterization of drought across Burkina Faso's 274,200 km^2 territory. Rather, these stations were selected specifically for their long-term data continuity and their distribution across the country's three main climatic zones (Sahelian, Sudano-Sahelian, Sudanian), making them representative reference points along the national climatic gradient rather than a dense spatial network capable of resolving sub-regional rainfall variability.

Consequently, the drought characterizations and trends reported here should be interpreted as indicative of station-level and zone-representative dynamics, not as spatially interpolated or basin-wide drought fields. This approach is consistent with common practice in data-scarce Sahelian contexts, where long, homogeneous synoptic records are prioritized over spatial density; nonetheless, future work integrating satellite-derived precipitation products (e.g., CHIRPS, TAMSAT) or a denser station network would help capture finer-scale spatial variability within each climatic zone.

4. Conclusions

This study characterized the spatio-temporal variability of historical meteorological droughts over the period 1981-2021, using the SPI-3 and SPEI-3 indices computed at nine synoptic stations representative of Burkina Faso's three climatic zones—Sahelian, Sudano-Sahelian, and Sudanian—and applied to the two key sub-seasonal windows of the rainy season: the early season (MJJ: May-June-July) and the late season (ASO: August-September-October).

The monthly time series analysis reveals three structurally distinct hydroclimatic phases. The period 1981-1990 was dominated by severe and extreme drought conditions, spatially coherent across all zones and both seasons, with the most persistent and intense signals concentrated in the Sahelian zone. The transitional period 1991-2010 was characterized by a partial but geographically differentiated rainfall recovery—the so-called Sahel greening—accompanied by the progressive emergence of evapotranspiration-driven water stress episodes that SPI-3 alone cannot detect. The post-2015 period exhibits a marked intensification of hydroclimatic variability, with rapid alternations between extreme dry and wet events occurring simultaneously across zones, consistent with a reconfiguration of the West African monsoon system under ongoing climate change.

The seasonal analysis of drought categories, frequency, and occurrence reveals a dual-mode structure in drought dynamics across Burkina Faso. The early rainy season (MJJ) constitutes the primary locus of drought occurrence under SPI-3, driven by the high interannual variability of monsoon onset—a vulnerability that directly threatens crop establishment and germination. The late rainy season (ASO), by contrast, experiences a systematically amplified drought signal under SPEI-3, particularly in the Sudanian zone, where cumulative thermal loading drives potential evapotranspiration to its seasonal peak by August-October, generating water stress that is invisible to precipitation-only monitoring. This seasonal asymmetry identifies two distinct agronomic vulnerability windows that require differentiated monitoring and early warning strategies. The frequency and duration analysis further demonstrates that SPEI-3 is the more comprehensive indicator for moderate and severe drought assessment, capturing the evapotranspiration-driven stress component that SPI-3 systematically misses, while SPI-3 retains superior sensitivity for detecting extreme drought episodes governed by catastrophic precipitation deficits. This index complementarity is not a methodological redundancy but a diagnostic necessity: in a warming semi-arid environment such as Burkina Faso, where rainfall variability remains the primary driver of drought but rising temperatures increasingly amplify evaporative demand, the joint use of both indices provides a fuller picture of hydroclimatic risk than either alone.

The trend and change point analysis reveals a predominantly positive long-term evolution in both SPI-3 and SPEI-3 across the Sahelian and Sudano-Sahelian zones, with significant increasing trends concentrated in ASO and structured around two clusters of structural change points: a first shift around 1997 marking the onset of the Sahelian rainfall recovery, and a second reinforcement around 2007-2009 reflecting the intensification of late-season precipitation documented by [45]. These positive trends are, however, spatially bounded: the Sudanian zone shows no significant trends in MJJ and no significant structural breaks under any index or season, indicating that the hydroclimatic reorganization observed since the mid-1990s remains a Sahelian and Sudano-Sahelian phenomenon that has not yet propagated to the southern sector of the country. Against this predominantly positive background, the isolated significant decreasing SPEI-3 MJJ trend at Fada Ngourma—the only negative significant trend in the entire dataset—constitutes a critical outlier, signaling that early-season moisture stress is intensifying at this station under rising evaporative demand even as rainfall trends remain neutral, a pattern that warrants targeted monitoring given its implications for rainfed agriculture in the eastern Sudano-Sahelian zone.

Several limitations should be acknowledged. The analysis is restricted to meteorological drought; propagation to agricultural and hydrological drought via soil moisture and streamflow was not addressed and warrants future investigation using SPEI-6 and SPEI-12. Land-use and land-cover changes, which significantly alter surface energy balance and runoff generation in the context of the Sahelian paradox [20] [21], were not incorporated into the drought attribution framework. Additionally, extending the station network to include hydrometric data would enable a joint meteorological-hydrological drought analysis consistent with the Nakanbé basin literature [7].

These findings carry direct operational relevance for drought risk management in Burkina Faso. SPEI-based monitoring should complement or replace SPI-only frameworks in national early warning systems, particularly given the thermal amplification documented here. Spatially differentiated adaptation strategies are required: water conservation and soil moisture management in the central and eastern sectors where evapotranspiration-driven drying trends are emerging, and investment in water storage infrastructure in the northern Sahelian zone where rainfall recovery is documented but early-season vulnerability persists. The compression of the effective growing season and the intensification of late-season water stress identified in this study could critically threaten millet, sorghum, and maize yields—the foundation of food security for a country where more than 80% of the population depends on rainfed agriculture. Integrating the intra-seasonal hydroclimatic dynamics characterized here—and in particular the SPI/SPEI divergence as a thermal amplification signal—into national agricultural planning, groundwater management frameworks, and surface water monitoring programs such as those currently underway in the Nakanbé basin represents an urgent and tractable priority for climate adaptation in the Sahel.

Acknowledgements

We gratefully acknowledge the PRSA (West Africa Food System Resilience Program) for providing financial support for our research.

Conflicts of Interest

The authors declare no conflicts of interest regarding the publication of this paper.

References

[1] Mbaye, M.L., Bodian, A., Kimambo, O.N., Rouamba, F.I. and Gaveta, E. (2021) Analyses of Past Extremes Precipitation-Evapotranspiration Indices over Sub-Saharan Countries. *Journal of Extreme Events*, **8**, Article ID: 2250002. https://doi.org/10.1142/s2345737622500026

[2] Peng, J., Dadson, S., Hirpa, F., Dyer, E., Lees, T., Miralles, D.G., *et al.* (2020) A Pan-African High-Resolution Drought Index Dataset. *Earth System Science Data*, **12**, 753-769. https://doi.org/10.5194/essd-12-753-2020

[3] Sarr, M., Moussa, A.M., Wade, M., Deme, E.H. and Diop, B. (2024) Regional Climate Models in the Simulation of the Drought of the 1970's and 1980's Years in Senegal (in West Africa). *Journal of Water Resource and Protection*, **16**, 585-604. https://doi.org/10.4236/jwarp.2024.169034

[4] Taylor, R.G., Todd, M.C., Kongola, L., Maurice, L., Nahozya, E., Sanga, H., *et al.* (2013) Evidence of the Dependence of Groundwater Resources on Extreme Rainfall in East Africa. *Nature Climate Change*, **3**, 374-378. https://doi.org/10.1038/nclimate1731

[5] Sogno, P., Klein, I. and Kuenzer, C. (2022) Remote Sensing of Surface Water Dynamics in the Context of Global Change—A Review. *Remote Sensing*, **14**, Article No. 2475. https://doi.org/10.3390/rs14102475

[6] Kingsford, R.T., Bino, G., Finlayson, C.M., Falster, D., Fitzsimons, J.A., Gawlik, D.E., *et al.* (2021) Ramsar Wetlands of International Importance-improving Conservation Outcomes. *Frontiers in Environmental Science*, **9**, Article ID: 643367. https://doi.org/10.3389/fenvs.2021.643367

[7] Fowé, T., Yonaba, R., Mounirou, L.A., Ouédraogo, E., Ibrahim, B., Niang, D., *et al.* (2023) From Meteorological to Hydrological Drought: A Case Study Using Standardized Indices in the Nakanbe River Basin, Burkina Faso. *Natural Hazards*, **119**, 1941-1965. https://doi.org/10.1007/s11069-023-06194-5

[8] Bambio, Y. (2013) Aid and Environment in Burkina Faso. WIDER Working Paper No. 2013/139, United Nations University World Institute for Development Economics Research (UNU-WIDER).

[9] Le, P.V.V., Phan-Van, T., Mai, K.V. and Tran, D.Q. (2019) Space-Time Variability of Drought over Vietnam. *International Journal of Climatology*, **39**, 5437-5451. https://doi.org/10.1002/joc.6164

[10] Li, J., Wang, Y., Li, Y., Ming, W., Long, Y. and Zhang, M. (2022) Relationship between Meteorological and Hydrological Droughts in the Upstream Regions of the Lancang-

Mekong River. *Journal of Water and Climate Change*, **13**, 421-433. https://doi.org/10.2166/wcc.2021.445

[11] Zhou, Z., Shi, H., Fu, Q., Ding, Y., Li, T. and Liu, S. (2021) Investigating the Propagation from Meteorological to Hydrological Drought by Introducing the Nonlinear Dependence with Directed Information Transfer Index. *Water Resources Research*, **57**, e2021WR030028. https://doi.org/10.1029/2021wr030028

[12] Hasan, H.H., Mohd Razali, S.F., Muhammad, N.S. and Ahmad, A. (2021) Hydrological Drought across Peninsular Malaysia: Implication of Drought Index. *Natural Hazards and Earth System Sciences Discussions*. https://doi.org/10.5194/nhess-2021-249

[13] Morid, S., Smakhtin, V. and Moghaddasi, M. (2006) Comparison of Seven Meteorological Indices for Drought Monitoring in Iran. *International Journal of Climatology*, **26**, 971-985. https://doi.org/10.1002/joc.1264

[14] Zargar, A., Sadiq, R., Naser, B. and Khan, F.I. (2011) A Review of Drought Indices. *Environmental Reviews*, **19**, 333-349. https://doi.org/10.1139/a11-013

[15] McKee, T.B., Doesken, N.J. and Kleist, J. (1993) The Relationship of Drought Frequency and Duration to Time Scales. *Proceedings of the* 8*th Conference on Ap-plied Climatology*, Anaheim, 17-22 January 1993, 179-183.

[16] Vicente-Serrano, S.M., Beguería, S. and López-Moreno, J.I. (2010) A Multiscalar Drought Index Sensitive to Global Warming: The Standardized Precipitation Evapotranspiration Index. *Journal of Climate*, **23**, 1696-1718. https://doi.org/10.1175/2009jcli2909.1

[17] Beguería, S., Vicente-Serrano, S.M., Reig, F. and Latorre, B. (2014) Standardized Precipitation Evapotranspiration Index (SPEI) Revisited: Parameter Fitting, Evapotranspiration Models, Tools, Datasets and Drought Monitoring. *International Journal of Climatology*, **34**, 3001-3023. https://doi.org/10.1002/joc.3887

[18] Yameogo, W.V.M., Kabore, O., Sanon, Z., Akpa, Y.L., Traore, F., Tankoano, B., *et al.* (2023) Dynamique spatio-temporelle des surfaces en eau du bassin du Nakanbé-Mané au Burkina Faso. *International Journal of Biological and Chemical Sciences*, **17**, 233-246. https://doi.org/10.4314/ijbcs.v17i1.17

[19] Gbohoui, Y.P., Paturel, J., Fowe, T., Karambiri, H. and Yacouba, H. (2021) Impacts des changements climatique et environnemental sur la réponse hydrologique du bassin du Nakanbé à Wayen (Burkina Faso) à travers le cadre de budyko. *Proceedings of the International Association of Hydrological Sciences*, **384**, 269-273. https://doi.org/10.5194/piahs-384-269-2021

[20] Yonaba, R., Biaou, A.C., Koïta, M., Tazen, F., Mounirou, L.A., Zouré, C.O., *et al.* (2021) A Dynamic Land Use/Land Cover Input Helps in Picturing the Sahelian Paradox: Assessing Variability and Attribution of Changes in Surface Runoff in a Sahelian Watershed. *Science of the Total Environment*, **757**, Article ID: 143792. https://doi.org/10.1016/j.scitotenv.2020.143792

[21] Yonaba, R., Mounirou, L.A., Tazen, F., Koïta, M., Biaou, A.C., Zouré, C.O., *et al.* (2024) Future Climate or Land Use? Attribution of Changes in Surface Runoff in a Typical Sahelian Landscape. *Comptes Rendus. Géoscience*, **355**, 411-438. https://doi.org/10.5802/crgeos.179

[22] Di Nunno, F., Yildiz, M.B. and Granata, F. (2025) Decoding the Architecture of Drought: SHAP-Enhanced Insights into the Climate Forces Reshaping the Sahel. Copernicus GmbH.

[23] Millogo, Z.N., Okogbue, E.C., Diasso, J.U., Ochei, M.C. and Sawadogo, W. (2025) Projection of Heatwave Characteristics over Burkina Faso under the Shared Socioeconomic Pathways Scenarios—SSP2-4.5 and SSP5-8.5. *Theoretical and Applied Cli-*

matology, **156**, Article No. 461. https://doi.org/10.1007/s00704-025-05676-9

[24] Ki, G.Z., Kébré, M.B., Somda, W., Gandema, S. and Dabilgou, F. (2026) Exploratory Data Analysis of Burkina Faso's Raw Daily Meteorological Records (1981-2021): Data Quality Insights and Potential Outlier Screening. *Environmental Research*: *Climate*, **8**, Article ID: 051012.

[25] Abramowitz, M. and Stegun, I.A. (1964) Handbook of Mathematical Functions with Formulas, Graphs, and Mathematical Tables. Applied Mathematics Series 55, National Bureau of Standards, Washington DC.

[26] Vonk, M.A. (2025) SPEI: A Python Package for Calculating and Visualizing Drought Indices. *Journal of Open Source Software*, **10**, Article No. 8454. https://doi.org/10.21105/joss.08454

[27] Xiong, X., Zhou, J., Liu, X. and Cui, Y. (2022). The Potential of Using Dynamic Surface Water Products for Drought Monitoring. *IGARSS* 2022-2022 *IEEE International Geoscience and Remote Sensing Symposium*, Kuala Lumpur, 17-22 July 2022, 6308-6311. https://doi.org/10.1109/igarss46834.2022.9884112

[28] Hamed, K.H. and Ramachandra Rao, A. (1998) A Modified Mann-Kendall Trend Test for Autocorrelated Data. *Journal of Hydrology*, **204**, 182-196. https://doi.org/10.1016/s0022-1694(97)00125-x

[29] Mann, H.B. (1945) Nonparametric Tests against Trend. *Econometrica*, **13**, 245-259. https://doi.org/10.2307/1907187

[30] Kendall, M.G. (1975) Rank Correlation Methods. 4th Edition, Charles Griffin.

[31] Sen, P.K. (1968) Estimates of the Regression Coefficient Based on Kendall's Tau. *Journal of the American Statistical Association*, **63**, 1379-1389. https://doi.org/10.1080/01621459.1968.10480934

[32] Pettitt, A.N. (1979) A Non-Parametric Approach to the Change-Point Problem. *Applied Statistics*, **28**, 126-135. https://doi.org/10.2307/2346729

[33] Hussain, M. and Mahmud, I. (2019) pyMannKendall: A Python Package for Non Parametric Mann Kendall Family of Trend Tests. *Journal of Open Source Software*, **4**, Article No. 1556. https://doi.org/10.21105/joss.01556

[34] Pohlert, T. (2023) trend: Non-Parametric Trend Tests and Change-Point Detection. R Package Version 1.1.6. https://CRAN.R-project.org/package=trend

[35] Militino, A.F., Moradi, M. and Ugarte, M.D. (2020) On the Performances of Trend and Change-Point Detection Methods for Remote Sensing Data. *Remote Sensing*, **12**, Article No. 1008. https://doi.org/10.3390/rs12061008

[36] Nicholson, S. (2005) On the Question of the "Recovery" of the Rains in the West African Sahel. *Journal of Arid Environments*, **63**, 615-641. https://doi.org/10.1016/j.jaridenv.2005.03.004

[37] Biasutti, M. (2019) Rainfall Trends in the African Sahel: Characteristics, Processes, and Causes. *WIREs Climate Change*, **10**, e591. https://doi.org/10.1002/wcc.591

[38] Sylla, M.B., Nikiema, P.M., Gibba, P., Kebe, I. and Klutse, N.A.B. (2016) Climate Change over West Africa: Recent Trends and Future Projections. In: Yaro, J.A. and Hesselberg, J., Eds., *Adaptation to Climate Change and Variability in Rural West Africa*, Springer International Publishing, 25-40. https://doi.org/10.1007/978-3-319-31499-0_3

[39] Fontaine, B., Gaetani, M., Ullmann, A. and Roucou, P. (2011) Time Evolution of Observed July-September Sea Surface Temperature-Sahel Climate Teleconnection with Removed Quasi-Global Effect (1900-2008). *Journal of Geophysical Research*, **116**, D04105. https://doi.org/10.1029/2010jd014843

[40] Stagge, J.H., Tallaksen, L.M., Gudmundsson, L., Van Loon, A.F. and Stahl, K. (2015) Candidate Distributions for Climatological Drought Indices (SPI and SPEI). *International Journal of Climatology*, **35**, 4027-4040. https://doi.org/10.1002/joc.4267

[41] Salack, S., Sarr, B., Sangare, S.K., Ly, M., Sanda, I.S. and Kunstmann, H. (2015) Crop-climate Ensemble Scenarios to Improve Risk Assessment and Resilience in the Semi-Arid Regions of West Africa. *Climate Research*, **65**, 107-121. https://doi.org/10.3354/cr01282

[42] Sivakumar, M.V.K. (1992) Empirical Analysis of Dry Spells for Agricultural Applications in West Africa. *Journal of Climate*, **5**, 532-539. https://doi.org/10.1175/1520-0442(1992)005<0532:eaodsf>2.0.co;2

[43] Zhao, T. and Dai, A. (2015) The Magnitude and Causes of Global Drought Changes in the Twenty-First Century under a Low-Moderate Emissions Scenario. *Journal of Climate*, **28**, 4490-4512. https://doi.org/10.1175/jcli-d-14-00363.1

[44] Lebel, T. and Ali, A. (2009) Recent Trends in the Central and Western Sahel Rainfall Regime (1990-2007). *Journal of Hydrology*, **375**, 52-64. https://doi.org/10.1016/j.jhydrol.2008.11.030

[45] Panthou, G., Lebel, T., Vischel, T., Quantin, G., Sane, Y., Ba, A., *et al.* (2018) Rainfall Intensification in Tropical Semi-Arid Regions: The Sahelian Case. *Environmental Research Letters*, **13**, Article ID: 064013. https://doi.org/10.1088/1748-9326/aac334

Appendix

Station	Zone	Index	Season	N years	MK Z	MK p-value	Sen slope (/decade)	Trend	Pettitt CP year	Pettitt p-value	Pettitt significant
Ouahigouya	Sahelian	SPI-3	MJJ	41	3.325	0.0009	0.4758	Increasing	1997	0.0037	Yes
Dori	Sahelian	SPI-3	MJJ	41	2.707	0.0068	0.3493	Increasing	1997	0.0222	Yes
Ouagadougou	Sudano-Sahelian	SPI-3	MJJ	41	2.86	0.0042	0.1077	Increasing	2008	0.0012	Yes
Dédougou	Sudano-Sahelian	SPI-3	MJJ	40	3.597	0.0003	0.2557	Increasing	1997	0.1823	No
Boromo	Sudano-Sahelian	SPI-3	MJJ	41	2.213	0.0269	0.3259	Increasing	2008	0.0337	Yes
Fada Ngourma	Sudano-Sahelian	SPI-3	MJJ	41	−0.194	0.8461	−0.0314	No trend	1995	0.9103	No
Bobo-Dioulasso	Sudanian	SPI-3	MJJ	41	0.685	0.4933	0.0929	No trend	1990	0.681	No
Gaoua	Sudanian	SPI-3	MJJ	41	0.213	0.831	0.0463	No trend	1984	0.6077	No
Pô	Sudanian	SPI-3	MJJ	41	0.988	0.3231	0.1285	No trend	1986	0.5876	No
Ouahigouya	Sahelian	SPI-3	ASO	41	3.381	0.0007	0.4677	Increasing	2007	0.0019	Yes
Dori	Sahelian	SPI-3	ASO	41	2.67	0.0076	0.259	Increasing	2009	0.0495	Yes
Ouagadougou	Sudano-Sahelian	SPI-3	ASO	41	4.208	0	0.5039	Increasing	2007	0.0046	Yes
Dédougou	Sudano-Sahelian	SPI-3	ASO	41	2.797	0.0052	0.3769	Increasing	1988	0.0359	Yes
Boromo	Sudano-Sahelian	SPI-3	ASO	41	1.101	0.271	0.0221	No trend	1993	0.4006	No
Fada Ngourma	Sudano-Sahelian	SPI-3	ASO	41	2.684	0.0073	0.4053	Increasing	1992	0.0123	Yes
Bobo-Dioulasso	Sudanian	SPI-3	ASO	41	1.674	0.0942	0.267	No trend	2014	0.1802	No
Gaoua	Sudanian	SPI-3	ASO	41	1.359	0.1741	0.2124	No trend	2018	0.5636	No
Pô	Sudanian	SPI-3	ASO	41	3.125	0.0018	0.2975	Increasing	1991	0.081	No
Ouahigouya	Sahelian	SPEI-3	MJJ	41	1.718	0.0857	0.2287	No trend	1991	0.0468	Yes
Dori	Sahelian	SPEI-3	MJJ	41	3.605	0.0003	0.4237	Increasing	1997	0.0021	Yes
Ouagadougou	Sudano-Sahelian	SPEI-3	MJJ	41	0.348	0.7277	0.0617	No trend	2008	0.3982	No
Dédougou	Sudano-Sahelian	SPEI-3	MJJ	38	1.621	0.1049	0.1648	No trend	1997	0.574	No
Boromo	Sudano-Sahelian	SPEI-3	MJJ	41	4.112	0	0.3757	Increasing	2008	0.017	Yes
Fada Ngourma	Sudano-Sahelian	SPEI-3	MJJ	41	−2.005	0.045	−0.2162	Decreasing	2010	0.3849	No
Bobo-Dioulasso	Sudanian	SPEI-3	MJJ	40	0.361	0.718	0.0425	No trend	2016	0.9599	No
Gaoua	Sudanian	SPEI-3	MJJ	41	−0.056	0.9552	−0.0015	No trend	1984	0.7427	No
Pô	Sudanian	SPEI-3	MJJ	37	0.719	0.4719	0.1366	No trend	1991	0.617	No
Ouahigouya	Sahelian	SPEI-3	ASO	41	3.201	0.0014	0.4512	Increasing	2007	0.0012	Yes
Dori	Sahelian	SPEI-3	ASO	41	2.976	0.0029	0.3875	Increasing	2009	0.0088	Yes
Ouagadougou	Sudano-Sahelian	SPEI-3	ASO	41	3.916	0.0001	0.4575	Increasing	2007	0.0142	Yes
Dédougou	Sudano-Sahelian	SPEI-3	ASO	38	2.791	0.0053	0.265	Increasing	2006	0.2117	No
Boromo	Sudano-Sahelian	SPEI-3	ASO	41	1.37	0.1706	0.1627	No trend	1993	0.3468	No
Fada Ngourma	Sudano-Sahelian	SPEI-3	ASO	40	2.587	0.0097	0.3726	Increasing	1992	0.0274	Yes
Bobo-Dioulasso	Sudanian	SPEI-3	ASO	38	4.001	0.0001	0.2676	Increasing	2014	0.1906	No
Gaoua	Sudanian	SPEI-3	ASO	41	1.438	0.1505	0.2133	No trend	2018	0.4264	No
Pô	Sudanian	SPEI-3	ASO	37	1.711	0.087	0.1705	No trend	1989	0.4204	No

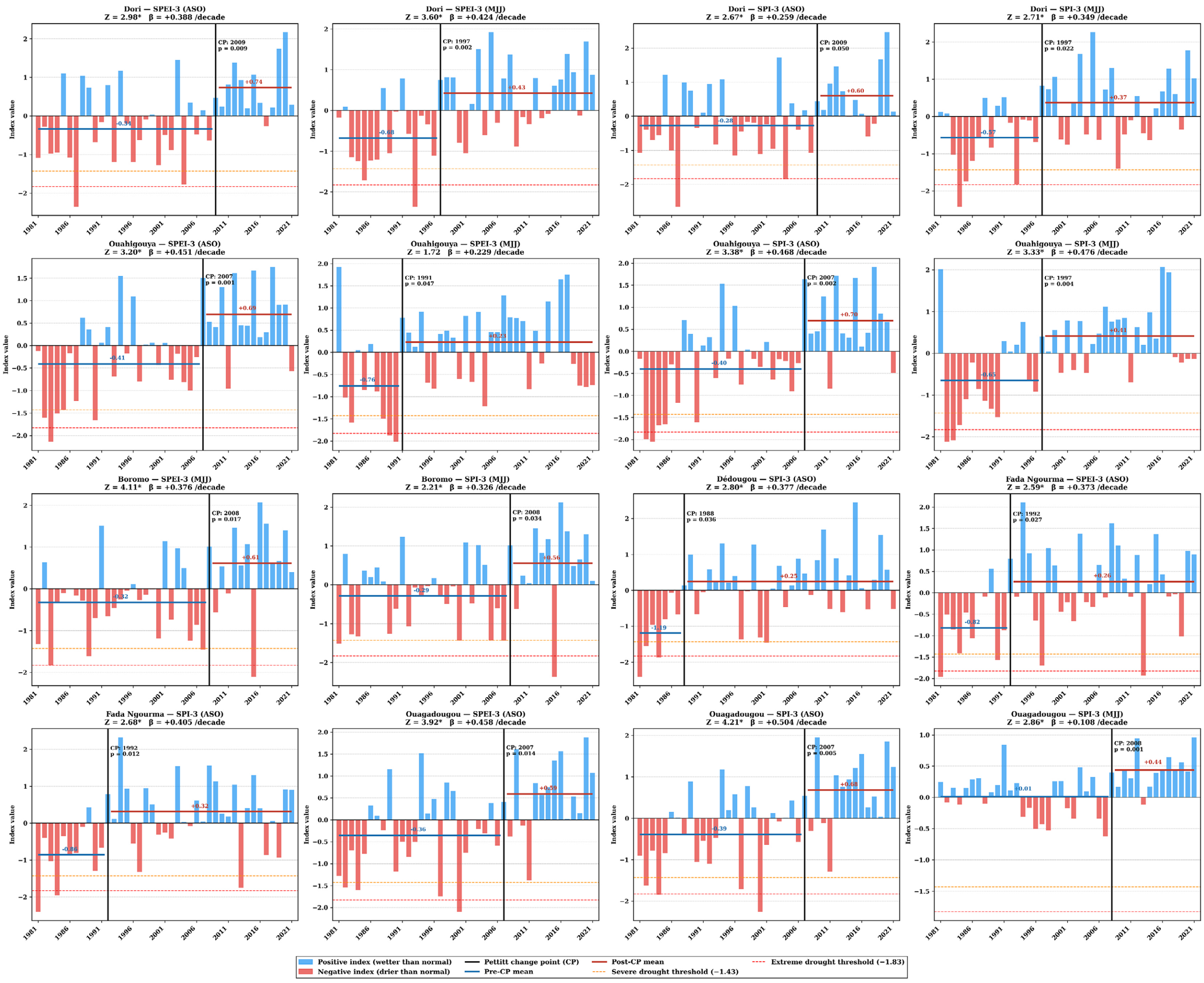

Figure S1. Annual SPI-3 and SPEI-3 time series for all station-index-season combinations exhibiting a statistically significant Pettitt change point ($p < 0.05$), Burkina Faso, 1981-2021. Blue bars indicate positive index values (wetter than normal); red bars indicate negative values (drier than normal). The vertical black line marks the Pettitt change point year (CP); the Pettitt p-value is indicated above the line. Horizontal lines show the pre-change point mean (blue) and post-change point mean (red), with numerical values annotated. Dashed orange and red horizontal lines indicate the severe drought threshold (SPI-3/SPEI-3 ≤ −1.43) and extreme drought threshold (SPI-3/SPEI-3 ≤ −1.83), respectively, following the classification of McKee *et al.* (1993) as adapted by WMO (2012). The Mann-Kendall Z-statistic (Hamed-Rao correction) and Sen's slope β (per decade) are reported in each panel title; asterisks (*) denote significance at $p < 0.05$. Panels are ordered by climatic zone (Sahelian, Sudano-Sahelian, Sudanian) and station name.